

Tomawac

Validation Manual

Thomas Awk

Version 7.2
December 29, 2016



AVERTISSEMENT / CAUTION

L'accès à ce document, ainsi que son utilisation, sont strictement limités aux personnes expressément habilitées par EDF.

EDF ne pourra être tenu responsable, au titre d'une action en responsabilité contractuelle, en responsabilité délictuelle ou de tout autre action, de tout dommage direct ou indirect, ou de quelque nature qu'il soit, ou de tout préjudice, notamment, de nature financier ou commercial, résultant de l'utilisation d'une quelconque information contenue dans ce document.

Les données et informations contenues dans ce document sont fournies "en l'état" sans aucune garantie expresse ou tacite de quelque nature que ce soit.

Toute modification, reproduction, extraction d'éléments, réutilisation de tout ou partie de ce document sans autorisation préalable écrite d'EDF ainsi que toute diffusion externe à EDF du présent document ou des informations qu'il contient est strictement interdite sous peine de sanctions.

The access to this document and its use are strictly limited to the persons expressly authorized to do so by EDF.

EDF shall not be deemed liable as a consequence of any action, for any direct or indirect damage, including, among others, commercial or financial loss arising from the use of any information contained in this document.

This document and the information contained therein are provided "as are" without any warranty of any kind, either expressed or implied.

Any total or partial modification, reproduction, new use, distribution or extraction of elements of this document or its content, without the express and prior written consent of EDF is strictly forbidden. Failure to comply to the above provisions will expose to sanctions.

Contents

1	Introduction	6
1.1	A word of caution	6
1.2	Validation layout	6
2	Presentation	8
2.1	General	8
2.2	Capabilities	8
2.2.1	Application domain of the model TOMAWAC	8
2.2.2	Wave interactions with other physical factors	9
2.2.3	The physical processes modelled in TOMAWAC	10
3	Validation	12
3.1	Evolution compared to the previous release	12
3.2	Difference with the previous validation	12
3.3	Next_Comput	13
3.3.1	Purpose	13
3.3.2	Description of the problem	13
3.3.3	Results	13
3.4	Triplets	14
3.4.1	Purpose	14
3.4.2	Description of the problem	14
3.5	Veget	16
3.5.1	Purpose	16
3.5.2	Description of the problem	16
3.5.3	Physical parameters	16
3.5.4	Geometry and Mesh	16
3.5.5	Initial and Boundary Conditions	16
3.5.6	Numerical parameters	16
3.5.7	Results	16
3.6	Bottom friction	18
3.6.1	Purpose	18
3.6.2	Description of the problem	18

3.6.3	Geometry and mesh	18
3.6.4	Numerical parameters	18
3.6.5	Initial and Boundary Conditions	18
3.6.6	Numerical parameters	18
3.6.7	Results	18
3.7	Dean	20
3.7.1	Purpose	20
3.7.2	Description of the problem	20
3.7.3	Reference	20
3.7.4	Physical parameters	20
3.7.5	Geometry and Mesh	20
3.7.6	Initial and Boundary Conditions	20
3.7.7	Numerical parameters	21
3.7.8	Results	21
3.8	Deferl_bj78	23
3.8.1	Purpose	23
3.8.2	Description of the problem	23
3.8.3	Physical parameters	23
3.8.4	Geometry and Mesh	23
3.8.5	Initial and Boundary Conditions	24
3.8.6	Numerical parameters	24
3.8.7	Results	24
3.8.8	Conclusion	26
3.9	Fetch Limited	27
3.9.1	Purpose	27
3.9.2	Reference experiments	28
3.9.3	Geometry of the domain and bathymetry	28
3.9.4	Initial and Boundary conditions	29
3.9.5	Numerical parameters	29
3.9.6	Results - infinite depth	29
3.9.7	Conclusion	35
3.10	Opposing current	40
3.10.1	Purpose	40
3.10.2	Description of the problem	40
3.10.3	Reference	40
3.10.4	Physical parameters	40
3.10.5	Geometry and Mesh	41
3.10.6	Initial and Boundary Conditions	41
3.10.7	Numerical parameters	41
3.10.8	Results	42
3.11	Shoal : Submerged elliptical mound	43
3.11.1	Purpose	43
3.11.2	Reference experiments	43
3.11.3	Test-case description	44
3.11.4	Numerical parameters	46
3.11.5	TOMAWAC Results	46
3.11.6	Conclusion	51

3.12 Turning wind	52
3.12.1 Purpose	52
3.12.2 Description of the problem	52
3.12.3 Physical parameters	52
3.12.4 Geometry and Mesh	52
3.12.5 Initial and Boundary Conditions	52
3.12.6 Numerical parameters	53
3.12.7 Results	53
3.13 Whirl current	55
3.13.1 Purpose	55
3.13.2 Description of the problem	55
3.13.3 Initial and Boundary Conditions	55
3.13.4 Geometry and Mesh	56
3.13.5 Numerical parameters	56
3.13.6 Results	56
3.13.7 Conclusion	57
Bibliography	61

1. Introduction

1.1 A word of caution

This document contains information about the quality of a complex modelling tool. Its purpose is to assist the user in assessing the reliability and accuracy of computational results, and to provide guidelines with respect to the applicability and judicious employment of this tool. This document does not, however, provide mathematical proof of the correctness of results for a specific application. The reader is referred to the License Agreement for pertinent legal terms and conditions associated with the use of the software.

The contents of this validation document attest to the fact that computational modelling of complex physical systems requires great care and inherently involves a number of uncertain factors. In order to obtain useful and accurate results for a particular application, the use of high-quality modelling tools is necessary but not sufficient. Ultimately, the quality of the computational results that can be achieved will depend upon the adequacy of available data as well as a suitable choice of model and modelling parameters.

1.2 Validation layout

This validation is presented hereafter using a *validation sheet form*, each sheet detailing the physical concepts involved, the physical and numerical parameters used and comparing both numerical and reference solutions. Then, each sheet displays the following informations:

- **Purpose & Problem description** : These first two parts give reader short details about the test case, the physical phenomena involved and specify how the numerical solution will be validated;
- **Reference** : This part gives the reference solution we are comparing to and explicits the analytical solution when available;
- **Physical parameters** : This part specifies the geometry, details all the physical parameters used to describe both porous media (soil model in particularly) and solute characteristics (dispersion/diffusion coefficients, soil \equiv pollutant interactions...);
- **Geometry and Mesh** : This part describes the mesh used in the TOMAWAC computation;
- **Initial and boundary conditions** : this part details both initial and boundary conditions used to simulate the case ;

- **Numerical parameters** : this part is used to specify the numerical parameters used (adaptive time step, mass-lumping when necessary...);
- **Results** : we comment in this part the numerical results against the reference ones, giving understanding keys and making assumptions when necessary.

2. Presentation

2.1 General

TOMAWAC is a scientific software which models the changes, both in the time and in the spatial domain, of the power spectrum of wind-driven waves and wave agitation for applications in the oceanic domain, in the intracontinental seas as well as in the coastal zone. The model uses the finite elements formalism for discretizing the sea domain; it is based on the computational subroutines of the TELEMAC system as developed by the EDF R&D's Laboratoire National d'Hydraulique et Environnement (LNHE). TOMAWAC is one of the models making up the TELEMAC system. The acronym TOMAWAC being adopted for naming the software was derived from the following English denomination:

TELEMAC-based Operational Model Addressing Wave Action Computation

TOMAWAC can be used for three types of applications:

- Wave climate forecasting a few days ahead, from wind field forecasts. This real time type of application is rather directed to weather-forecasting institutes such as Météo-France, whose one mission consists in predicting continuously the weather developments and, as the case may be, publishing storm warnings.
- Hindcasting of exceptional events having severely damaged maritime structures and for which field records are either incomplete or unavailable.
- Study of wave climatology and maritime or coastal site features, through the application of various, medium or extreme, weather conditions in order to obtain the conditions necessary to carry out projects and studies (harbour constructions, morphodynamic coastal evolutions, ...).

2.2 Capabilities

2.2.1 Application domain of the model TOMAWAC

TOMAWAC is designed to be applied from the ocean domain up to the coastal zone. The limits of the application range can be determined by the value of the relative depth d/L , wherein d denotes the water height (in metres) and L denotes the wave length (in metres) corresponding to the peak spectral frequency for irregular waves.

The application domain of TOMAWAC includes:

- **the oceanic domain**, characterized by large water depths, i.e. by relative water depths of over 0.5. The dominant physical processes are: wind driven waves, whitecapping dissipation and non-linear quadruplet interactions.
- **the continental seas and the medium depths**, characterized by a relative water depth ranging from 0.05 to 0.5. In addition to the above processes, the bottom friction, the shoaling (wave growth due to a bottom rise) and the effects of refraction due to the bathymetry and/or to the currents are to be taken into account.
- **The coastal domain**, including shoals or near-shore areas (relative water depth lower than 0.05). For these shallow water areas, such physical processes as bottom friction, bathymetric breaking, non-linear triad interactions between waves should be included. Furthermore, it could be useful to take into account the effects related to unsteady sea level and currents due to the tide and/or to the weather-dependent surges.

Through a so-called finite element spatial discretization, one computational grid may include mesh cells among which the ratio of the largest sizes to the smallest ones may reach or even exceed 100. That is why TOMAWAC can be applied to a sea domain that is featured by highly variable relative water depths; in particular, the coastal areas can be finely represented.

The application domain of TOMAWAC does not include the harbour areas and, more generally, all those cases in which the effects of reflection on structures and/or diffraction may not be ignored.

A first version of a diffraction model is available in TOMAWAC and is able to represent some diffraction effects. The model presents still some limits. It is highly recommended to use phase-resolving models when a detailed simulation of diffraction effects is required (e.g. harbor agitation).

2.2.2 Wave interactions with other physical factors

Several factors are involved in the wave physics and interact to various extents with the waves changing their characteristics. The following main factors should be mentioned:

- bathymetry and sea bottom geometry (bottom friction, refraction, surf-breaking, non-linear effects of interactions with the bottom, sand rippling...)
- atmospheric circulation (wind and pressure effects)
- tide pattern (variation of currents and water heights),
- three-dimensional oceanic circulation currents,
- over/underelevations caused by exceptional weather events, resulting in sea levels variations up to several meters (storm, surges).

The fine modelling of the interactions between these various physical factors and the waves is generally rather complex and several research projects are currently focused on it. Within the application domain as defined in the previous paragraph, TOMAWAC models the following interactions:

- **wave-bathymetry interaction**: the submarine relief data input into TOMAWAC are constant in time, but the sea level can change in time. In addition to the effects of the sea level variations in time, TOMAWAC allows to take into account refraction, shoaling, bottom friction and bathymetric breaking. TOMAWAC simulations can take into account some diffraction effects.

- **wave-atmosphere interaction:** this interaction is the driving phenomenon in the wave generation, takes part in energy dissipation processes (whitecapping, wave propagation against the wind...) and is involved in the energy transfer. To represent the unsteady behaviour of this interaction, TOMAWAC requires 10 m wind fields (specification of the couple of horizontal velocity components) with a time step matched to the weather conditions being modelled. These wind fields can be provided either by a meteorological model or from satellite measurements.
- **wave-current interaction:** the sea currents (as generated either by the tide or by oceanic circulations) may significantly affect the waves according to their intensity. They modify the refractive wave propagation direction, they reduce or increase the wave height according to their propagation direction in relation to the waves and may influence the wave periods if exhibiting a marked unsteady behaviour. In TOMAWAC, the current field is provided by the couple of horizontal components of its average (or depth-integrated) velocity at the nodes of the computational grid. TOMAWAC allows to model the frequency changes caused either by the Doppler effect or by the unsteady currents, as well as by an heterogeneous current field.

2.2.3 The physical processes modelled in TOMAWAC

Those interactions being taken into account by TOMAWAC have been reviewed and a number of physical events or processes have been mentioned in the previous paragraph. These processes modify the total wave energy as well as the directional spectrum distribution of that energy (i.e. the shape of the directional spectrum of energy). So far, the numerical modelling of these various processes, although some of them are now very well known, is not yet mature and keep on providing many investigation subjects. Considering the brief review of physical interactions given in the previous paragraph, the following physical processes are taken into account and digitally modelled in TOMAWAC:

—> **Energy source/dissipation processes:**

- wind driven interactions with atmosphere. Those interactions imply the modelling of the wind energy input into the waves. It is the prevailing source term for the wave energy directional spectrum. The way that spectrum evolves primarily depends on wind velocity, direction, time of action and fetch (distance over which the wind is active). It must be pointed out that the energy which is dissipated when the wind attenuates the waves is not taken into account in TOMAWAC.
- whitecapping dissipation or wave breaking, due to an excessive wave steepness during wave generation and propagation.
- bottom friction-induced dissipation, mainly occurring in shallow water (bottom grain size distribution, ripples, percolation...)
- dissipation through bathymetric breaking. As the waves come near the coast, they swell due to shoaling until they break when they become too steep.
- dissipation through wave blocking due to strong opposing currents.

—> **Non-linear energy transfer conservative processes:**

- non-linear resonant quadruplet interactions, which is the exchange process prevailing at great depths.
- non-linear triad interactions, which become the prevailing process at small depths.

—> Wave propagation-related processes:

- wave propagation due to the wave group velocity and, in case, to the velocity of the medium in which it propagates (sea currents).
- depth-induced refraction which, at small depths, modifies the directions of the wave-ray and then implies an energy transfer over the propagation directions.
- shoaling: wave height variation process as the water depth decreases, due to the reduced wavelength and variation of energy propagation velocity.
- current-induced refraction which also causes a deviation of the wave-ray and an energy transfer over the propagation directions.
- interactions with unsteady currents, inducing frequency transfers (e.g. as regards tidal seas).
- diffraction by a coastal structure (breakwater, pier, etc...) or a shoal, resulting in an energy transfer towards the shadow areas beyond the obstacles blocking the wave propagation. The current version of the diffraction model implemented in TOMAWAC is able to represent qualitatively some diffraction effects.

It should be remembered that, due to the hypothesis adopted in paragraph 2.2.1 about the TOMAWAC application domain, the reflection (partial or total) from a structure or a pronounced depth irregularity is not addressed by the model.

3. Validation

3.1 Evolution compared to the previous release

Beside some bugs corrected from the previous version, we can denote two main new phenomena that are now modelled.

- **Strong dissipation through wave blocking due to strong opposing currents.** When water waves meet a strong adverse current, with a velocity that approaches the wave group velocity, waves are blocked. Two options can be now considered in TOMAWAC to take into account wave blocking effects. The first one considers an equilibrium range spectrum (in the presence of ambient flow) applied as an upper limit for the spectrum [11]. The second one add a dissipative term on the right-hand side of the action balance equation [8]. This leads to one test case *called opposing_current* that tests the two options.
- **Dissipation due to vegetation.** When the ratio between vegetation height and water depth is important, vegetation can imply some dissipation. Some methods exist to modelize this dissipation. The method we chose is based on the formulation proposed by Suzuki et al. [20]. This functionnality leads to 2 new test cases called *dean* and *veget*. The first one is a realistic simulation with a Fortran user file, the second one is less realistic but without any Fortran user file.

3.2 Difference with the previous validation

In this validations we have extended in some cases the number of options for a given tested functionnality. For example, in deferl_bj78, we do not only test Battle and janssen but two other models are tested. In fetch_limited, 3 others configurations are tested. Another test case has been added named Triplets, to test dissipation due to triplet interactions according to two different models.

Another difference is the use of automatic graphics that are added to this documentation. Though we kepted the old graphics that were comparing to some experimental data.

3.3 Next_Comput

3.3.1 Purpose

The aim of this case is to test a computation that follows another one. We start from a calculated state at a time and we simulate some new time step.

3.3.2 Description of the problem

The simulation is the same as the shoal test case so one will read that test case for physical description. We start here from a shoal simulation until time 600s. The result of this previous simulation is inside the file indicated by the keyword *PREVIOUS COMPUTATION FILE (FICHIER DU CALCUL PRECEDENT* in french). This file has been created by adding the keyword *GLOBAL RESULT FILE (FICHIER DES RESULTATS GLOBAUX* in french) in the shoal steering case. We simulate for 600 other seconds. We can compare the result to the one obtained by shoal test case with 1200 seconds of simulation.

3.3.3 Results

After 600 s, the difference with the full shoal simulation is null.

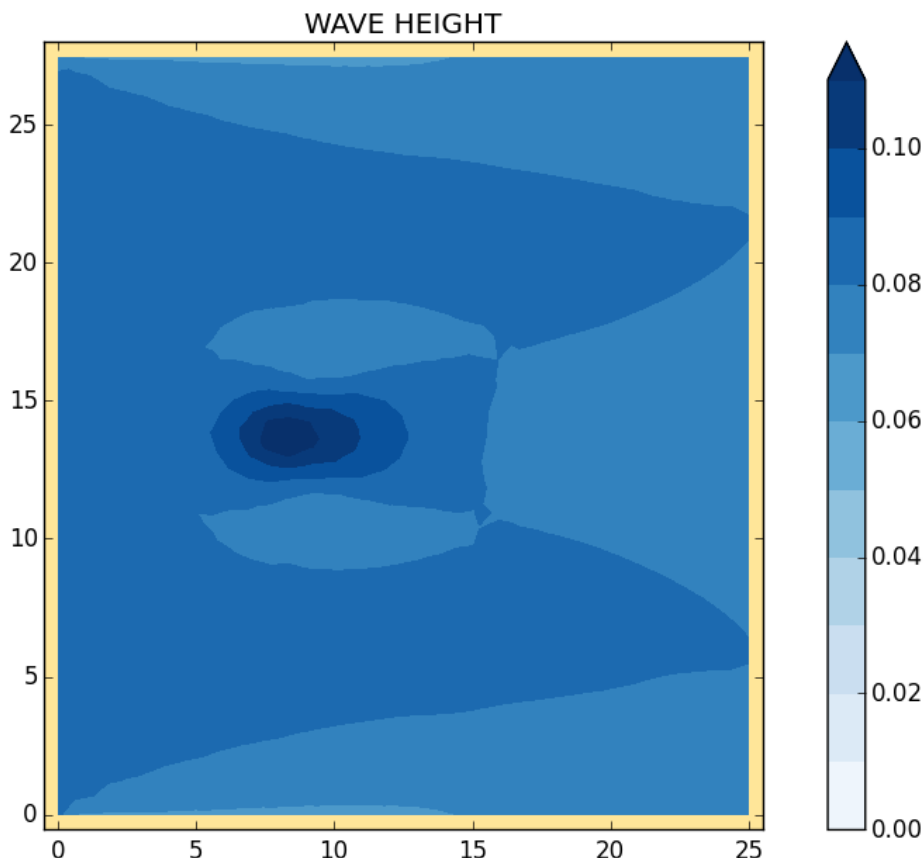


Figure 3.1: Wave height HM0

3.4 Triplets

3.4.1 Purpose

This test case has been created to test the extend the covering by using option of triad interactions that were not used in other cases.

3.4.2 Description of the problem

We simulate non linear transfers between triads. In the first case we use Lumped Triad Approximation model (LTA) and in the second case we use the SPB model

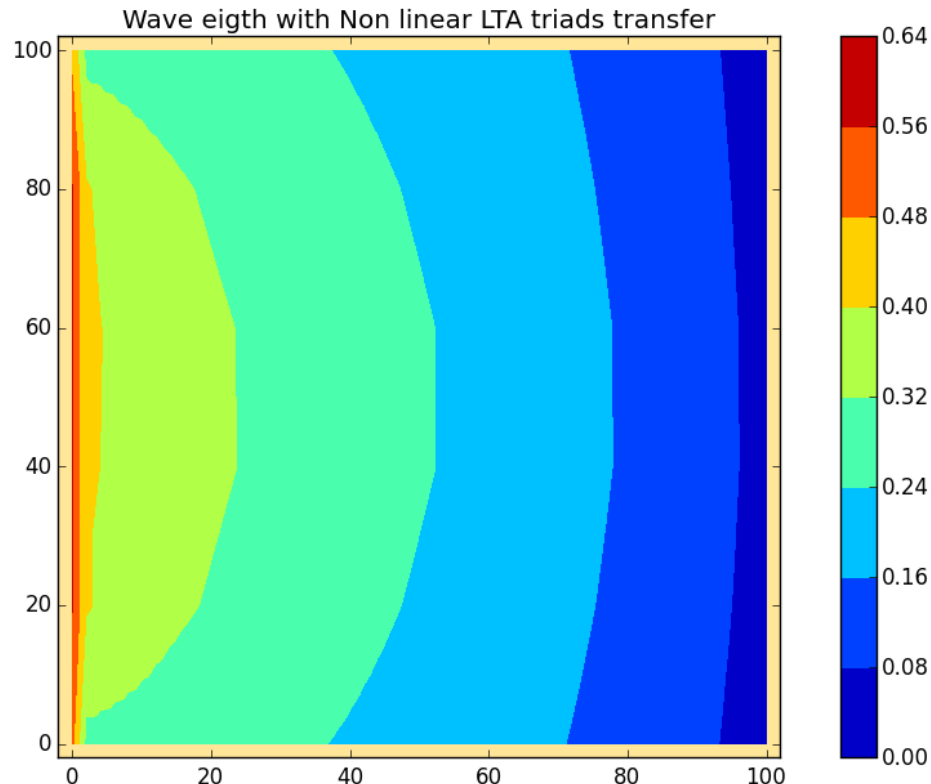


Figure 3.2: Wave height for Lumped Triad Approximation model

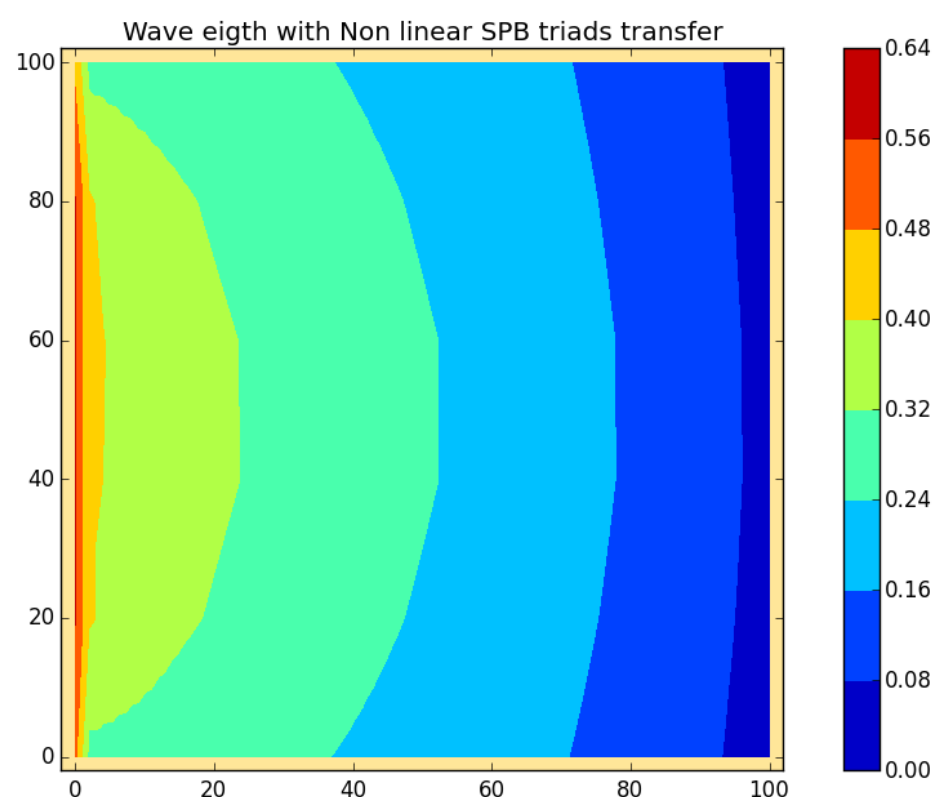


Figure 3.3: Wave height for SPB model

3.5 Veget

3.5.1 Purpose

This test case has been created to test the vegetation dissipation without any fortran user. That is only a test that checks non regression solution. It refers to the model of [21] but since the frequency is not monochromatic the result can not be compared to the results they obtained.

3.5.2 Description of the problem

We simulate the dissipation due to vegetation in a channel.

The random wave transformation model for a flat bottom by Mendez and Losada (2004) is expressed as follows.

$$H_{rms} = \frac{H_{rms,0}}{1 + \tilde{\beta}x}$$

with

$$\tilde{\beta} = \frac{1}{3\sqrt{\pi}} \tilde{C}_D b_v H_{rms,0} k \frac{\sinh^3 k\alpha h + 3 \sinh k\alpha h}{(\sinh 2kh + 2kh) \sinh kh}$$

where $H_{rms,o}$ is the value of root mean square wave height at the wave boundary $x=0$.

3.5.3 Physical parameters

Simulations were carried out with a water depth $h = 2.0$ m and root mean square wave height $H_{rms,o}$ (0.4 m) at the incident wave boundary. The vegetation height was taken as equal to the water depth ($\alpha h = 2.0m$), the plant area per unit height was $b_v = 0.04m$, the number of plants per unit area was $N = 10units/m^2$, and the bulk drag coefficient was $\tilde{C}_D = 1.0$. The vegetation was present in the entire computational domain.

3.5.4 Geometry and Mesh

The computational domain was composed of a flat (slope = 0.0) 2D grid with an aspect ratio of 1 (cross-shore direction):10 (along shore direction). The calculation grid size was set as 2.0 m in the wave propagation direction. There are 906 nodes and 1500 triangles.

3.5.5 Initial and Boundary Conditions

The initial significative height is 0.015m with an initial frequency of 1 Hz and an initial peak factor of 3.3 and a mean direction of 90° and a initial directionnal spread of 0. The boundary conditions are given by a jonswap spectrum with a boundary pic factor of 3.3Hz a significative height of 0.5656m and a boundary frequency pic of 1

3.5.6 Numerical parameters

The time step was of 0.1s and the duration of the computation of 480s. The spectro-angular mesh has 36 directions and 6 frequencies. The frequential ratio was of 1.01 and the minimum frequency of 0.0951Hz.

3.5.7 Results

We do not compare results with an experiment as the choice of not having any fortran user prevent from being in the same condition but [3] obtained good result agreements when comparing to [21]

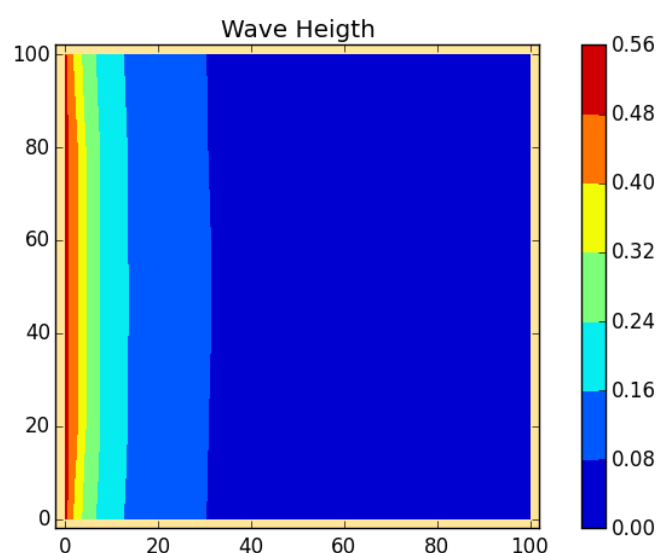


Figure 3.4: Wave height HM0

3.6 Bottom friction

3.6.1 Purpose

This test case aims at testing the effect of friction coefficients used in Tomawac, one acting upon energy whereas the other one acts upon the mean directional frequency. This test case is an inheritance of a comparison between Cowadis and Tomawac. There is no measure to validate the test, it is only a non regression testing.

3.6.2 Description of the problem

The waves are let freely propagate in a large body of water. The swell should loose some energy and its frequency should change only under the effect of friction bottom (the boundary conditions may be ignored because the domain is very wide).

The expression that is used for computing the friction in Tomawac is as follows :

$$Q_{bf}(\theta, \omega) = -\Gamma \left(\frac{\sigma}{g \cdot \sinh(kd)} \right) F(\theta, \omega) \quad (3.1)$$

Where Γ , the BOTTOM_FRICTION_COEFFICIENT, is taken equal to 0.038, its default value.

3.6.3 Geometry and mesh

The computational domain is a 100 km by 25 km rectangle and the flat bottom elevation is taken equal to 5m.

The mesh is made with 492 nodes (80 on the boundary) and 902 triangles.

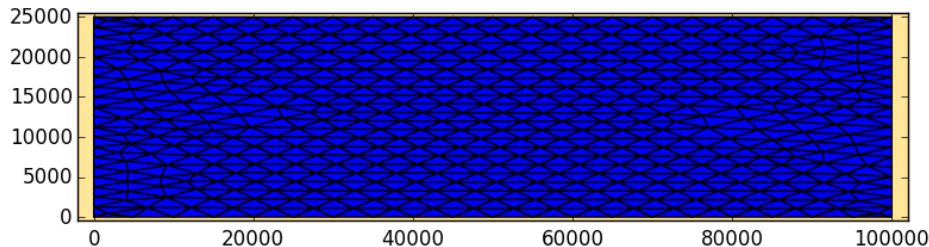


Figure 3.5: mesh of the domain

3.6.4 Numerical parameters

Time duration is 30000 s, time step is equal to 100 s, the spectro-angular mesh has 24 angles and 25 frequencies spread on a geometric progression common ratio 1.1 with a minimum of 0.056447393.

3.6.5 Initial and Boundary Conditions

For both conditions, we take a Jonswap spectrum with a 1 m significant wave height, a peak frequency of 0.1. The angular distribution function follows a $\cos^2 \theta$ distribution with an angular spreading of 6 and a mean direction of 0.

3.6.6 Numerical parameters

3.6.7 Results

In this case we just verify that we still have the same results as the ones obtained during the comparison with Cowadis [19].

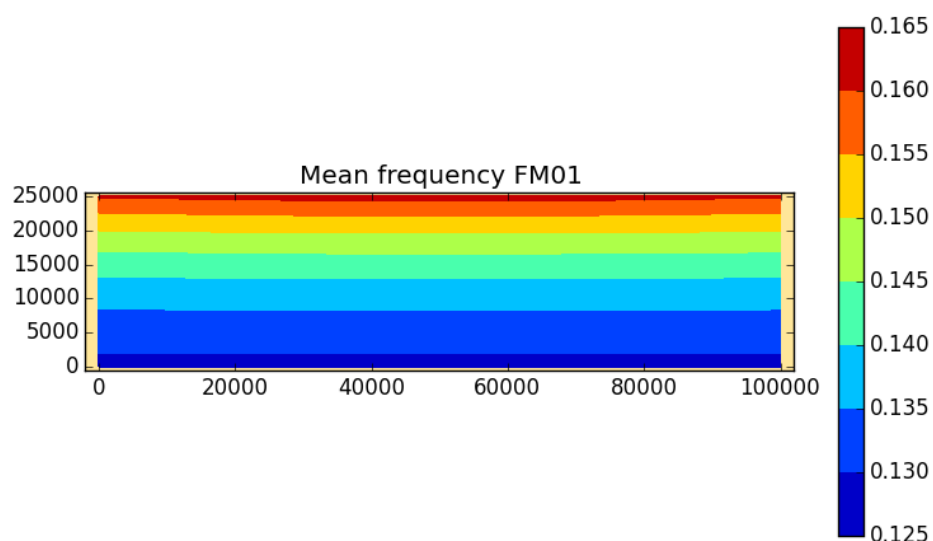


Figure 3.6: WAVE HEIGHT HM0

3.7 Dean

3.7.1 Purpose

This test case aims to verify the development made to take into account the wave energy dissipation induced by vegetation. When the ratio between vegetation height and water depth is important, dissipation may become non negligible.

3.7.2 Description of the problem

In order to carry out an analysis of the influence of plant height, vegetation field width and breaking on waves propagation, Mendez and Losada (2004) analysed the evolution of the wave height over a Dean's shape profile [7] defined as follows:

$$h = 0.25(300 - x)^{\frac{2}{3}}$$

Where h [m] is the water depth, 0.25 the sediment scale parameter, and $x=0$ is the offshore boundary.

3.7.3 Reference

In this test case the prediction of the effects of vegetation is validated with the original equation and results from Mendez and Losada [21]. The reference file *fom_dean.slf* contains the results that have been compared to [21] in [3].

3.7.4 Physical parameters

Two vegetation heights, $dv = 1$ m and 3 m and a single 100 m long vegetation field, from 50 to 150 m, are used. The number of plants per square meter is $N = 20 \text{ units/m}^2$ and the plant area per unit height of vegetation is $b_v = 0.25 \text{ m}$. The bulk drag coefficient is 0.2. All these parameters are set in the Fortran user subroutine *QVEG*

3.7.5 Geometry and Mesh

The computational domain was composed of a flat (slope = 0.0) 2D grid with an aspect ratio of 1 (cross-shore direction):10 (along shore direction). The calculation grid size was set as 2.0 m in the wave propagation direction. Bathymetry and mesh are shown on figure 3.7. There are 906 nodes and 1500 triangles.

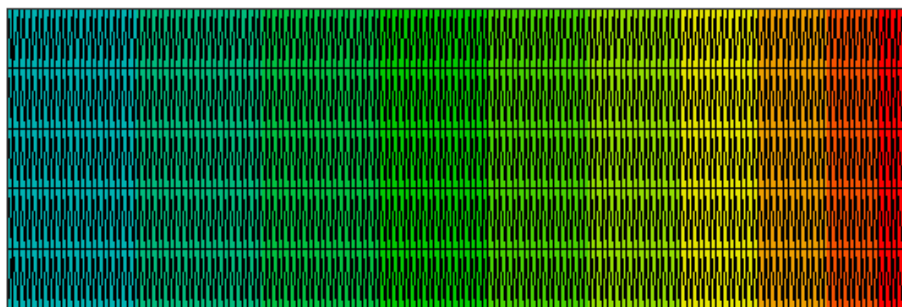


Figure 3.7: depth evolution

3.7.6 Initial and Boundary Conditions

According to the authors, the incident wave conditions imposed to TOMAWAC on the offshore boundary are given by $H_{rms,o} = 2.5 \text{ m}$ (equivalent to significant wave height $H_s = 3.54 \text{ m}$) and

$T_p = 10$ s. The incident waves are uni-directional random waves as defined in the previous section and the breaking model used is that of Thornton and Guza (1983) with $\gamma = 0.6$ (where the parameter γ is the proportional control factor indicating the maximum water depth “Hm” compatible with water depth “d”:).

The significant initial wave height was taken equal to 3.54 m with a peak frequency of 2.2 Hz. The angular distribution function follows a $\cos^{2s} \theta$ distribution with an angular spreading of 2, and a mean direction of 90.

3.7.7 Numerical parameters

The time step is of 0.1 s and the duration of the computation of 480 s. The spectro-angular mesh has 36 directions and 6 frequencies. The frequential ratio is of 1.01 and the minimum frequency of 0.0951 Hz. The frequencies are filtered to keep only the fourth one (0.1 Hz) at 90 degrees to respect the $T_p = 10$ s imposed to the boundaries.

The spectrum tail factor was taken at 4.

3.7.8 Results

The results from Mendez and Losada and TOMAWAC model are compared in Fig. 3.8 below. Even if the test case is made with 1 m of vegetation, we present on Figure 3.8 the results obtained for three different height of vegetation, 0 m, 1 m and 3 m [3]. The results show very good agreement between the Mendez and Losada model [21] and TOMAWAC. We notice that differences seem very small and we can thus conclude that TOMAWAC is able to reproduce the same wave attenuation as with the random wave transformation model for breaking unidirectional random waves.

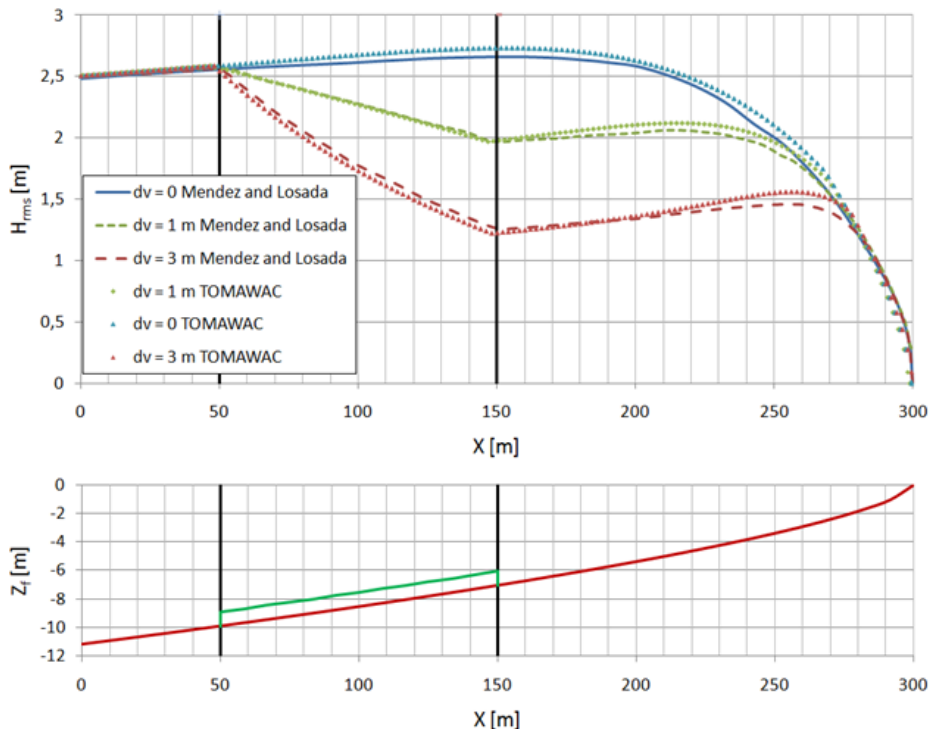


Figure 3.8: Comparison of H_{rms} evolution for numerical wave model (TOMAWAC) and random wave transformation model (Mendez and Losada) over Dean’s shape profile.

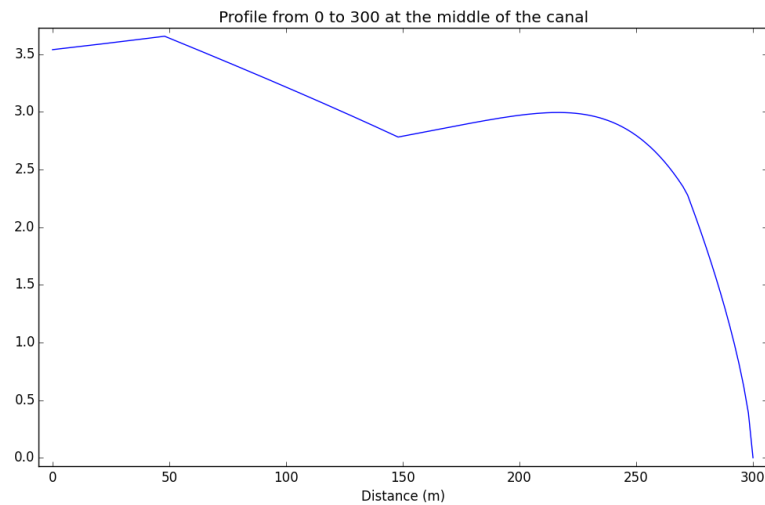


Figure 3.9: Wave height for the last calculation ($dv=1m$)

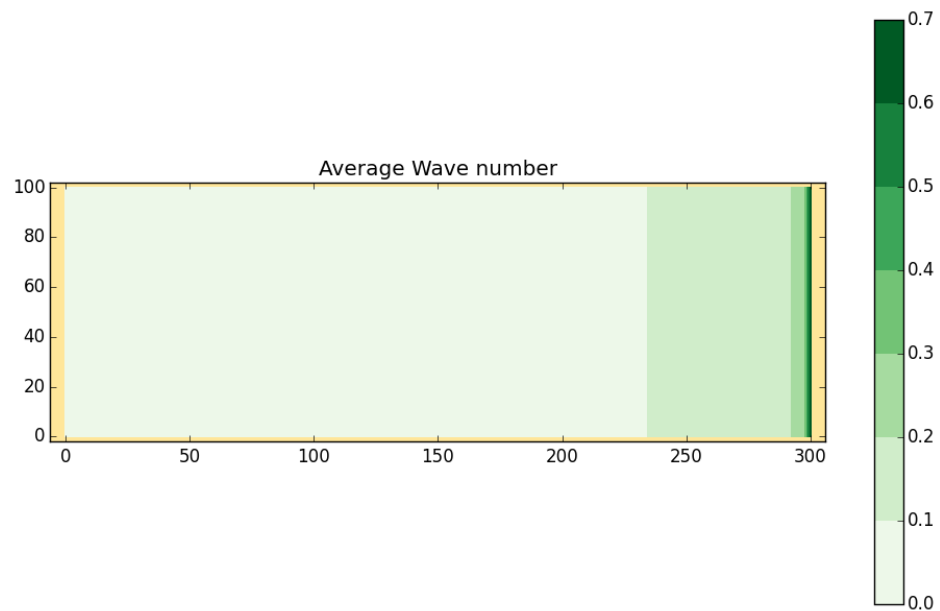


Figure 3.10: Average Wave number ($dv=1m$)

3.8 Deferl_bj78

3.8.1 Purpose

The aim of this case is to test the modelisation of depth-induced breaking. The results are compared to laboratory data [2]

3.8.2 Description of the problem

Our test case corresponds to the “run 15” in Battjes and Janssen [2]. It is a rectilinear beach with a bar. The bathymetry of that beach varies as shown on Figure 3.11. The Battjes and Janssen’s breaking model is used :

$F_1 = \int_{\theta=0}^{2\pi} F_0(\theta) d\theta$ where $F_0(\theta)$ is the first moment of the action density spectrum over frequency.

$$\frac{dF_1}{dt} = -\alpha_1 Q_b \omega_1 \frac{H_m^2}{8\pi}$$

wherein H_m denotes the maximum wave height. Q_b , the fraction of breaking waves or breaking rate and α_1 a numerical constant of order of 1.

H_m is given by a relationship that is derived from de Miche’s criterion:

$$H_m = \frac{\gamma_1}{k_1} \tanh \left(\frac{\gamma_2 k_1 d}{\gamma_1} \right)$$

wherein k_1 is related to ω_1 by the dispersion relationship.

Q_b is assessed, according to the Battjes and Janssen’s theory as the solution of the implicit equation:

$$\frac{1 - Q_b}{\ln Q_b} = -\frac{8F_1}{H_m^2}$$

The “directionnal” version of that source term is based on the assumption that the breaking does not change the directionnal distribution of energy. The source term writes :

$$Q_{br}(f, \theta) = -\frac{\alpha Q_b f_c H_m^2}{4} \frac{F(f, \theta)}{m_0}$$

The values of numerical constants α_1 , γ_1 et γ_2 as prescribed by Battjes and Janssen are 1, 0.88 and 0.8 respectively. These values, however can and must be matched as a function of the camber of incident waves and bottom slope. To that purpose the following keyword are provided : *DEPTH-INDUCED BREAKING 1 (BJ) COEFFICIENT ALPHA* for α_1 , *DEPTH-INDUCED BREAKING 1 (BJ) COEFFICIENT GAMMA1* for γ_1 and *DEPTH-INDUCED BREAKING 1 (BJ) COEFFICIENT GAMMA2* for γ_2 .

3.8.3 Physical parameters

The Battjes and Janssen’s experiments were conducted in a channel and in signle-direction wave conditions. We have then taken a little directionnal spread(s=32) in order to set up similar condition.

3.8.4 Geometry and Mesh

The domain is a 25 m by 12 m rectangle. The depth is constant over y and varrying with x as shown on Figure 3.11

The mesh is free, it is made of 648 triangles and 373 points. The boundary has 96 points.

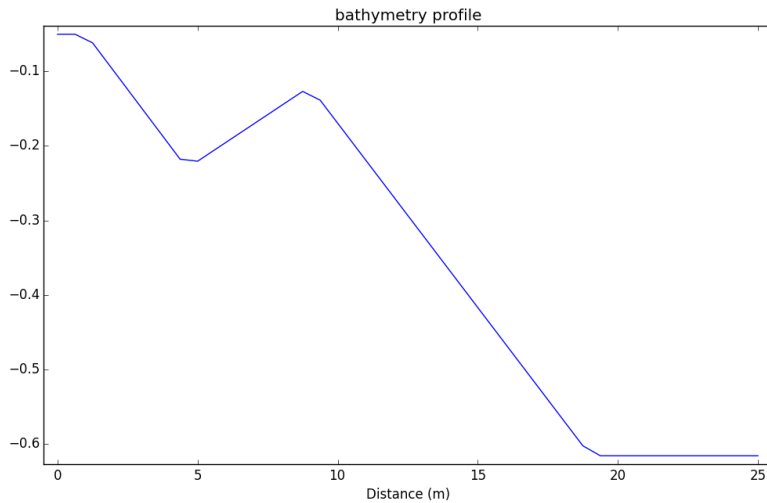


Figure 3.11: section depth

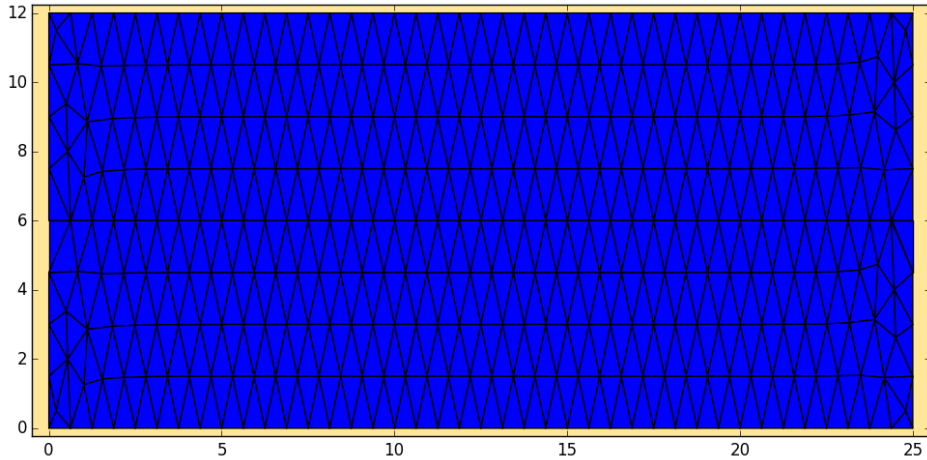


Figure 3.12: mesh of the domain.

3.8.5 Initial and Boundary Conditions

The initial spectrum is null.

As for the boundary conditions, a Pierson-Moskowitz-typed spectrum is prescribed at the west of the domain with a boundary peak frequency of 0.53Hz, a significative height of 0.202 m and a boundary peak factor of 3.3. The boundary principal direction is 270.

3.8.6 Numerical parameters

The time duration is 35 s with a time step of 0.35 s, the spectro-angular mesh has 24 angles and 25 frequencies spread on a geometric progression common ratio 1.1 with a minimum of 0.168874

3.8.7 Results

Figure 3.13 displays the significant wave heights as computed by Tomawac. One can see that Tomawac results are quite similar to the laboratory data.

The effect of wave breaking on the mean frequency is not taken into account in this case of

Tomawac. As we suppose that energy dissipation does not affect the spectro-angular energy spread. The energy transfers of the pre-breaking are not taken into account.

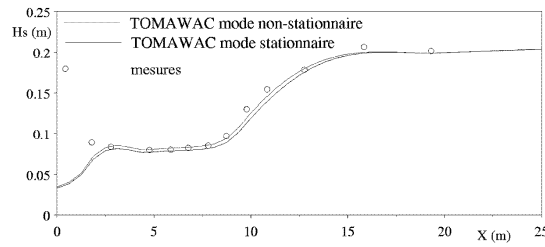


Figure 3.13: comparison of the significative wave heigths

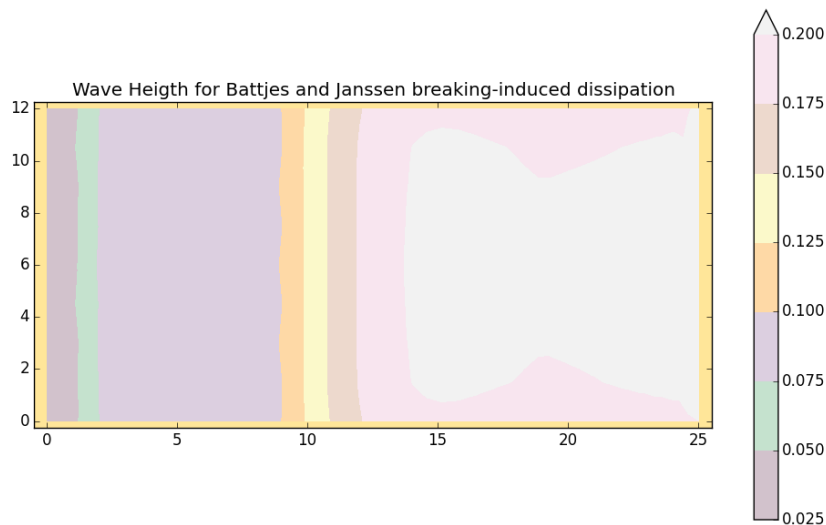


Figure 3.14: Significative wave heigths for Battjes and Janssen Model

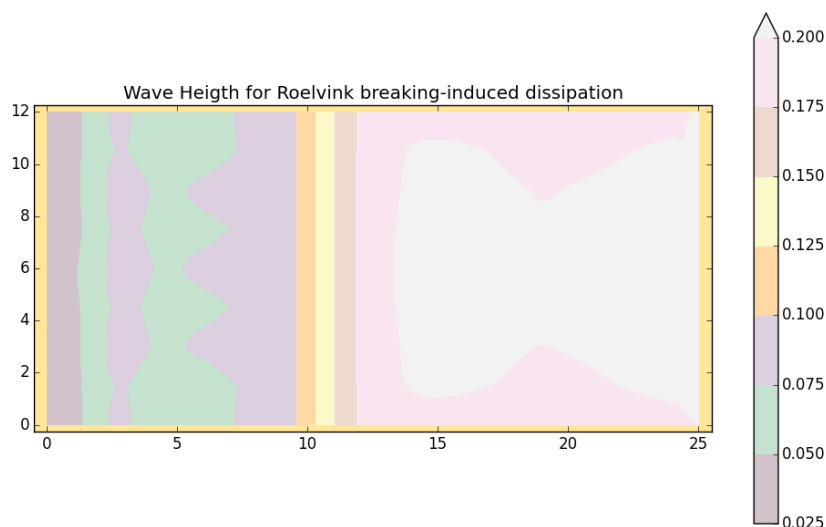


Figure 3.15: Significative wave heigths for Roelvink's model

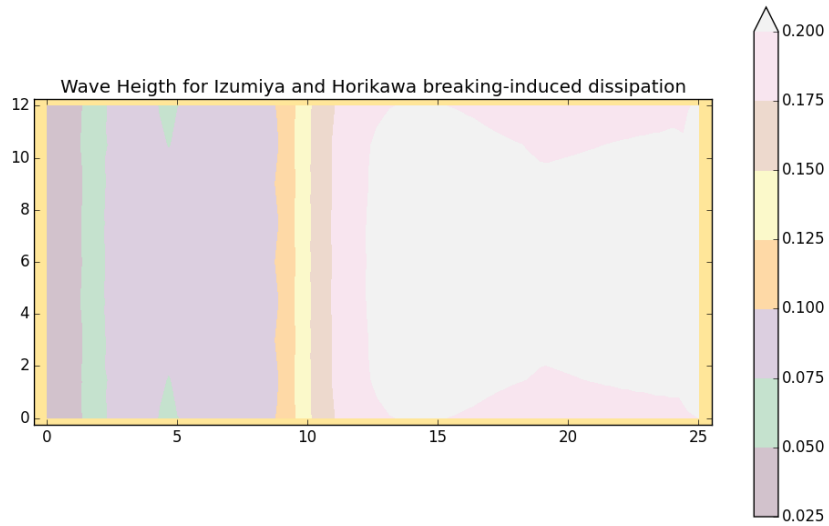


Figure 3.16: Significative wave heigths for Izumiya and Horikawa's turbulence model

3.8.8 Conclusion

The breaking induced dissipation of energy is properly represented in Tomawac. The effect on the mean frequency can be neglected.

Models	Wind generation model	white capping model	Quadruplet transfers formula	Depth	Bottom friction coeff.	Depth-induced breaking dissipation model
test 1	Janssen [22] [23]	Komen [14] Janssen; [23]	DIA*	inf	—	—
test 2	Snyder [25]	Komen ; Janssen	DIA	inf	—	—
test 3	Snyder	Westhuyzen [26]	DIA	inf	—	—
test 4	Yan ([15])	Westhuyzen	DIA	inf	—	—
test 5	Snyder	Westhuyzen	Exact GQM** coarse discretization	inf	—	—
test 6	Janssen	Komen ; Janssen Janssen	Exact GQM coarse discretization	inf	—	—
test 6b	Janssen	Komen ; Janssen	Exact GQM medium discretization	inf	—	—
test 7a	Snyder	Westhuyzen	DIA	180	0.038	—
test 7b	Snyder	Westhuyzen	DIA	60	0.038	—
test 7c	Snyder	Westhuyzen	DIA	30	0.038	—
test 7d	Snyder	Westhuyzen	DIA	15	0.038	—
test 7e	Snyder	Westhuyzen	DIA	5	0.038	Battjes & Janssen (V = 20m/s)

Table 3.1: Different models used for this test-case. In all cases, linear wave growth term from the formula of Cavalieri and Malanotte-Rizzoli (1981) is used.* : *Discrete Interaction Approximation,Hasselmann et al., 1985.* ** : *Gaussian Quadrature Method,introduced by Lavrenov [13] and implemented by Benoit and Gagnaire-Renou [9]*

3.9 Fetch Limited

3.9.1 Purpose

The goal of this test-case is to validate the generation (Source/sink terms) and the growth of the wave spectrum depending of the length of wind action (fetch) with a constant wind defined at 10 meters from the sea surface. The domain used is simple and we want to observe the evolution of few parameters along its length, as the significant wave height, peak period and variance spectrum. It is supposed that the wind blew long enough to have reached a steady state.

Thus, this benchmark will allow us to compare and validate the different models of wind generation (three models), whitecapping dissipation (two models), non-linear quadruplet interactions (three models but only two are used here). Friction bottom dissipation and eventually depth-induced breaking dissipation (four models) is also included when a finite depth is imposed. The models used are presented in the Table 3.1.

3.9.2 Reference experiments

In order to validate TOMAWAC results, they will be compared to different empirical formulas:

- Infinite depth :

JONSWAP [10]

CERC (1977) [5]

Wilson and Goda [28]

Kahma and Calkoen [4]

- Finite depth:

CERC (1984)[6]

3.9.3 Geometry of the domain and bathymetry

Domain dimension: 1000 km * 500 km

test 7a 180 m

test 7b 60 m

test 7c 30 m

test 7d 15 m

test 7e 5 m

or infinite

Depth constant along the domain:

Mesh

Several meshes have been tested. The important point highlighted by the analysis is that at the begining of the fetch the mesh must be sufficiently fine. At the end, the "free" mesh has been kept because it is the most used in industry and maritime applications (can be adapted to coast).

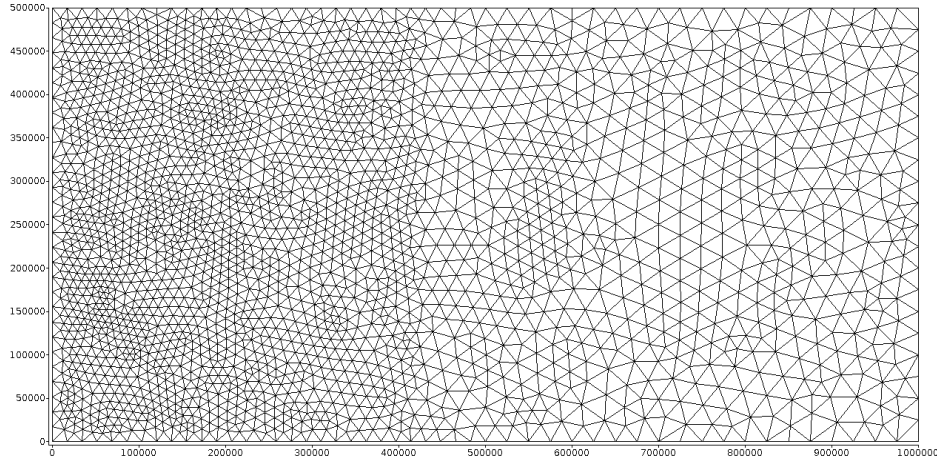


Figure 3.17: Free and refined mesh $\Delta x_{bigger} \approx 25000m$ - $\Delta x_{medium} \approx 20000m$ - $\Delta x_{smaller} \approx 10000m$

Spectro-angular discretization

- 50 frequencies ($f_1 = 0.04$ Hz for $U_{10} = 20$ m/s, $f_1 = 0.08$ Hz for $U_{10} = 10$ m/s with geometric spacing $q = 1.05$)
- 36 directions uniformly distributed

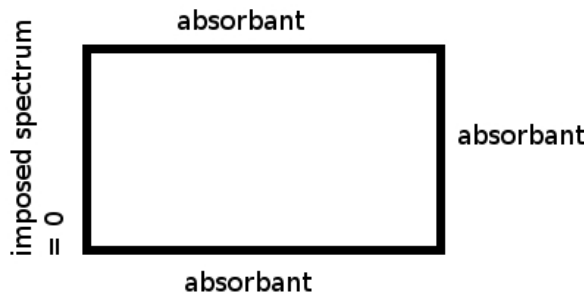


Figure 3.18: Boundary conditions

3.9.4 Initial and Boundary conditions

Jonswap spectrum has been set as initial condition.

The domain is a part of a sea. A constant and homogeneous wind blows perpendicular to a long and straight coastline. The boundary conditions are shown in Figure 3.18:

3.9.5 Numerical parameters

- time step : 900 s
- physical time reached : 48 h
- characterization of the computer :

Core : Linux 2.6.32-5-amdb64

Processors : Intel(R) xeon(R) CPU E5620 @ 2.4Ghz

• CPU times :	tests 1/2/3/4	test 5/6	tests 6b	tests 7
CPU times	3 min	3h25	5h40	25 s

3.9.6 Results - infinite depth

Wave growth depending on the fetch for different wind velocities.

Figure 3.19 shows the significant wave heights and the peak periods of waves along the fetch (along the axis $y = 250 \text{ m}$) for the test 1 (the others are not shown because they give the same conclusions). These curves are obtained after 48 hour of wind action for a wind of 5 to 25 m/s. It is clearly seen that the wind has a considerable impact on these values and bigger waves are obtained with stronger wind. Also, stronger is the wind, longer is the fetch needed to reach the steady state. It can be noticed that the significant wave height does not grow linearly but following the squared wind velocity.

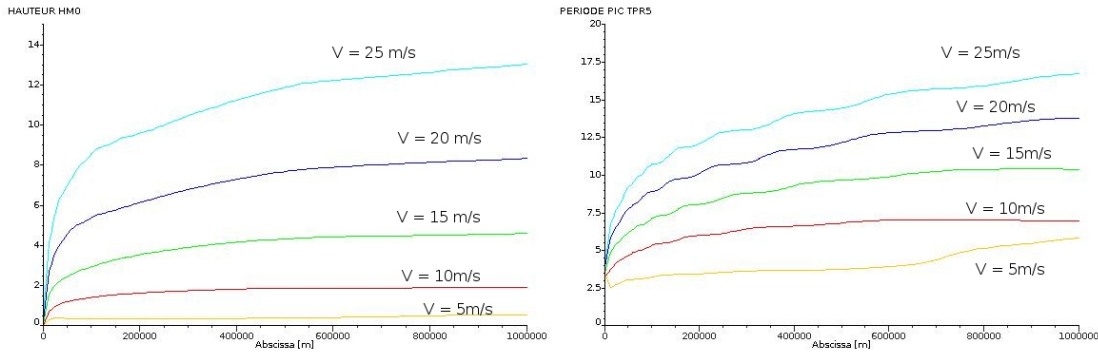


Figure 3.19: Significant wave heights and peak periods for the first test, $U_{10} = 5 - 10 - 15 - 20 - 25 \text{ m/s}$

Non-dimensionnal variances and peak frequencies.

Here all the tests are compared, but only with a 20 m/s and 10 m/s winds. The values obtained with TOMAWAC V6P2 are compared with the empirical formulas : JONSWAP [10], CERC (1977)[5], Wilson [28], Kahma [4]. The non-dimensional variables are :

- Non-dimensional Fetch : $x* = \frac{gx}{U_{10}^2}$
- Non-dimensional variance : $m_0* = \frac{g^2 m_0}{U_{10}^4}$
- Non-dimensional peak frequency : $f_p* = \frac{U_{10} f_p}{g}$

Where U_{10} is the wind velocity at 10 meters from the sea.

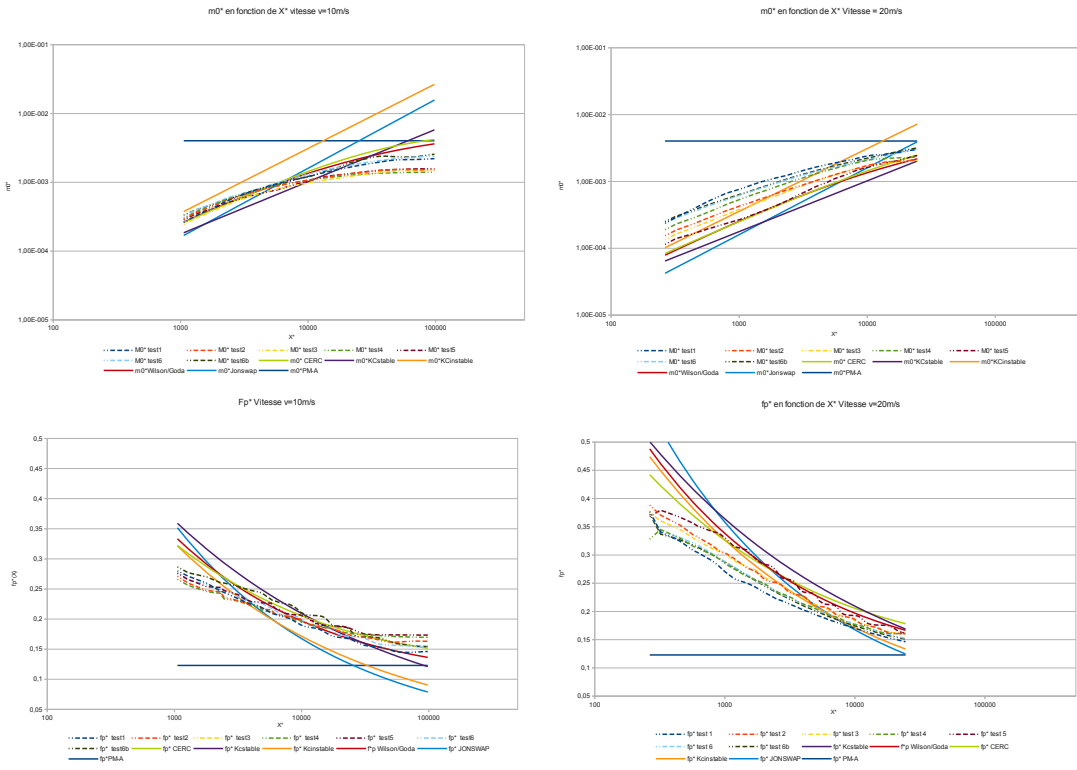


Figure 3.20: Comparaison de la variance normalisée $M0^*$ et de la fréquence de pointe normalisée fp^* pour $U_{10} = 10\text{m/s}$ (gauche) et 20m/s (droite), $m0^*$ MP-A et fp^* PM-A sont, respectivement, la variance et la fréquence de pointe limite donnée par la formule revisée de Pierson-Moskowitz de Alves [1]

Figure 3.20 shows the different results obtained. Generally, all tests give correct results, and stay close to the CERC, Wilson & Goda and Kahma & Calkoen curves.

The wind impact can be seen by two different behaviours. Indeed, for a 10 m/s wind, the results are really close to the empirical formula at small fetches. As the fetch grows, the differences between the models increrase, and the curves began to stray from the empirical formulas. In this case, the models of tests 1, 6 and 6b give the best results. At 20 m/s, a different behaviour is noticed: at small fetch the results are quite different from the empirical curves and it is only when the fetch grows that they match well with the empirical formula. In this case it is the model of test 5 which gives the best results. It can be concluded that there is a range where TOMAWAC results are really correct whatever the models used. For strong winds, an exact resolution of the quadruplet transfers, Snyder's wind generation model and Westhuyzen white capping model (test 5) give better results at small fetch.

Thus, the analysis of Figure 3.20 shows a good matching between the TOMAWAC wave simulations and the empirical formulas. A comparison was also done with the revisited Pierson-Moskowitz asymptotic limits from Alves and Banner [1] for fully developed wind waves, the U_{10} -scaled asymptotes is added on Figure 3.20. The formula gives:

$$\varepsilon = (4.02 \pm 0.62) * 10^{-3}$$

$$v = (1.23 \pm 0.08) * 10^{-1}$$

It seems that the non-dimensional peak frequency f_p^* is a little bit over-estimated and the non-dimensional variance is a bit underestimated. Indeed, the empirical formula given by CERC

(1984), which is used as a criterion for fully developed seas, to calculate the minimum fetch during the minimum duration (48h), is : $\frac{t_{min}g}{U_{10}} = 68.8 \left(\frac{X_{min}g}{U_{10}^2} \right)^{0.67}$. Applying this formula we found that the fully developed seas are reached around 1117 km for a 10 m/s wind and around 1672km for a 20 m/s wind. Thus, the fully developed sea may not be entirely reached at our last point ($X_{10} = 1000km$), which may explain the growth of the variance spectrum for some of the tests (see next subsection).

Variance spectrum for a constant wind.

In this subsection, we look at the development of the variance spectrum $E(f)$ along the fetch.

$$E(f) = \int_0^{2\pi} F(f, \theta) d\theta$$

The spectra are worked out for different points of fetch and for two wind speeds (10 m/s and 20 m/s):

Points	fetch
Point 1	25 km
Point 2	50 km
Point 3	100 km
Point 4	150 km
Point 5	200 km
Point 6	300 km
Point 7	400 km
Point 8	800 km
Point 9	750 km
Point 10	1000 km

Dimensional variance spectrum (not shown here) gives correct results with a big growth of the peak value with the wind.

The non-dimensional frequency is defined by: $f_* = \frac{U_{10} * f}{g}$.

and the variance spectra are normalised by the peak value of the Pierson-Moskowitz spectrum, which corresponds to the steady state:

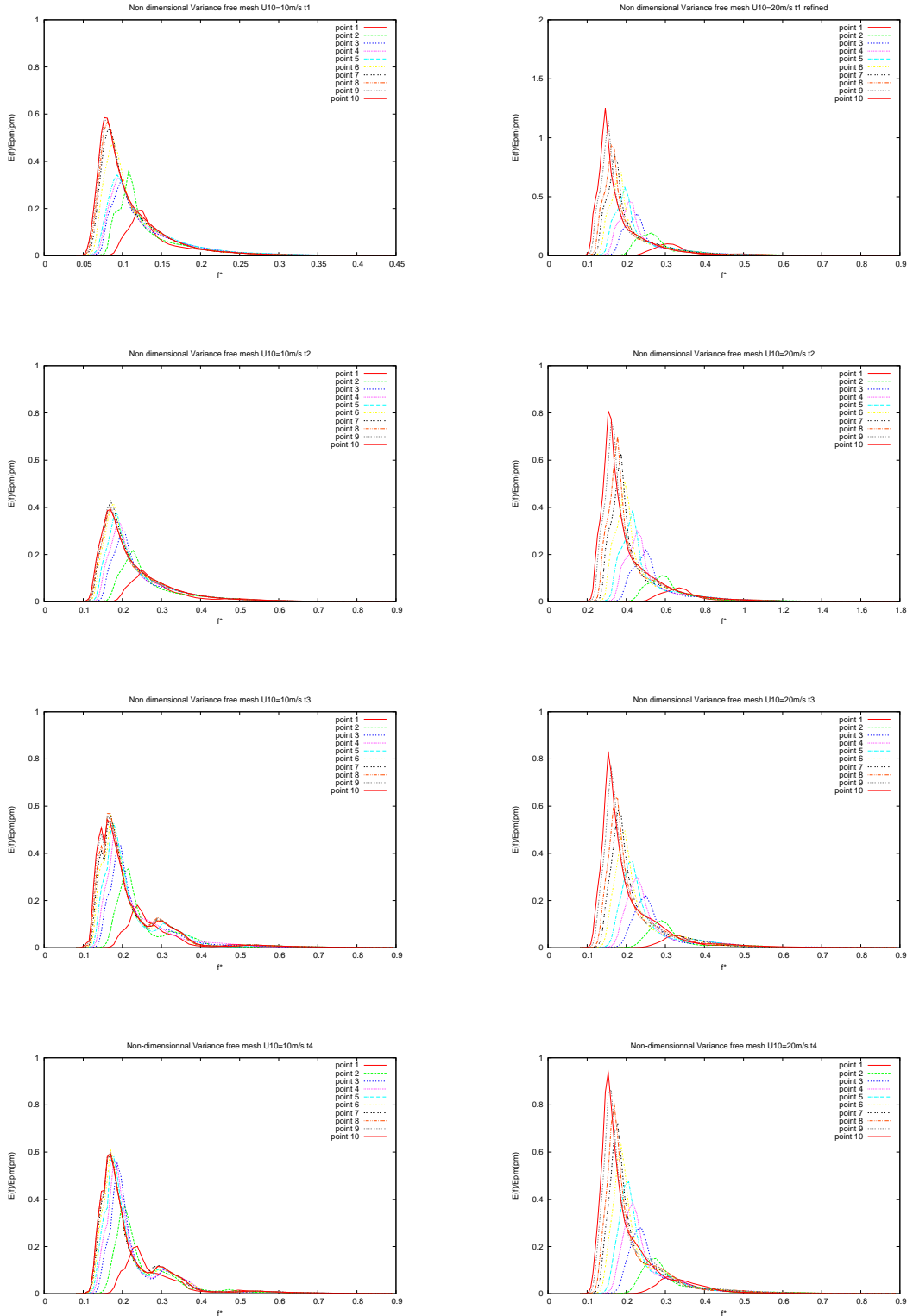
$$E_{PM}(f_{PM}) = \frac{\alpha g^2}{(2\pi)^4 f_{PM}^5} \exp(-5/4) \text{ with } f_{PM} = \frac{0.13g}{U_{10}} \text{ and the Philipp's constant } \alpha = 0.0081$$

On Figure 3.21, non-dimensional variance spectra can be observed. We can notice that as the fetch grows, the variance spectrum amplitude grows and the peak frequency declines. Moreover, the variance spectrum tends to the Pierson-Moskowitz spectrum for some cases. The exact quadruplet transfers calculation impact can be seen on the test 5, 6 and 6b, the shape of the curve changes, the spectrum is more peaked and the maximum value is higher, and it allows to observe a spectrum peak overstepping the state value predicted by Pierson-Moskowitz formula, it is an overshoot (test 6 for $U_{10} = 20m/s$ and test 6b).

For $U_{10} = 10m/s$, the last fetch points (points 7, 8, 9 and 10) get really close spectra. We can conclude that from a certain fetch, the fully developed sea state is reached. Althought, for the case $U_{10} = 20m/s$, the spectrum continues to grow and the overshoot's presence shows that this balance state is not yet reached. Thus, TOMAWAC gives good results which can be improved with the exact GQM quadruplet transfers model.

Finite depth TOMAWAC results

In this subsection, finite depths are considered : 180 m, 60 m, 30 m, 15 m and 5 m. In regards of Miche's criterion (1994), excepted for a 5 meters depth and $V = 20 m/s$, there is no bathymetric breaking dissipation. All the tests are done for the same generation (Snyder), white capping



(Westhuysen) and quadruplet transfer (DIA) models. Figure 3.22 shows the evolution of the non-dimensional variance along the fetch for the different tests. In order to compare with the CERC (1984) parametrization, non-dimensional variables are defined as:

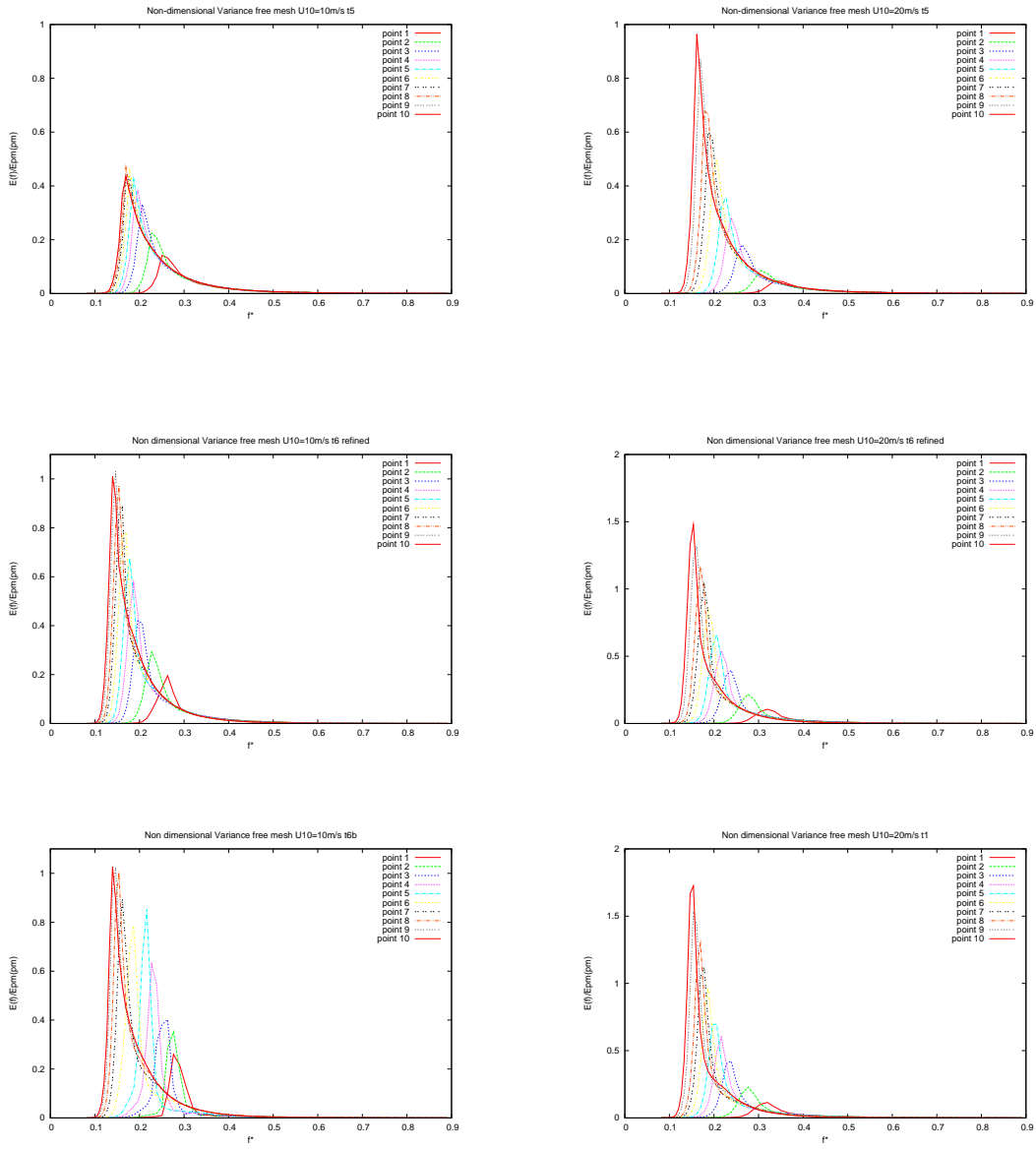


Figure 3.21: Comparison of normalized spectrum variance for the different tests and $U_{10} = 10\text{m/s}$ (left) and 20m/s (right).

- CERC parametrization (1984) :

$$X* = \frac{g*X}{U_a}$$

$$U_a = 0.71 * U_{10}^{1.23}$$

$$m0* = \frac{g^2*m0}{U_a^4}$$

It can be noticed that the non-dimensional variance decreases with depth. Indeed, bottom friction effects are more important at small depths. On the contrary, the peak frequency grows when the depth increases because the friction has more impact on small frequency waves, which leads to a growth of the peak frequency.

On Figure 6, we can see that for a 20 m/s wind, TOMAWAC curves are really matching with the CERC (1984) forecasting, particularly for $d = 15 - 30 - 60\text{ m}$. Indeed, it is advised in CERC publication to use their model for a depth between 15 and 90 meters. But the results are still good for $d = 180\text{ m}$ and $d = 5\text{ m}$.

For a 10m/s wind, except for $d = 5\text{ m}$ and $d = 15\text{ m}$, the results are less close to the CERC curves. At small fetches, TOMAWAC results are overvalued, and at large fetches, they are undervalued. In CERC publication (1984), it is advised to use an infinite model for depth over 90m. So the CERC infinite depth model (1977) is added to the graphs and we can see that the results are closer to it for a 10 m/s wind and $d \geq 30\text{m}$. For a 20 m/s wind, at $d = 180\text{m}$ and at large fetches, TOMAWAC results tends to the infinite depth limit. Generally, TOMAWAC gives correct results if you adapt the good model at the application.

3.9.7 Conclusion

Infinite Depth

This benchmark allows to verify that TOMAWAC results for simultaneous processing of different source terms are correct. A comparison with empirical formulas validates this simulation with generally matching results. The use of the exact GQM quadruplet transfers model allows the visualization of overshoots, but CPU time are increased, so it is not advisable to use this model for big industrial cases.

Finite depth

Even if a 1000 km fetch with only 5 m depth is hard to study in reality, TOMAWAC results get close to the empirical formula. Bottom friction effect seems to be well represented.

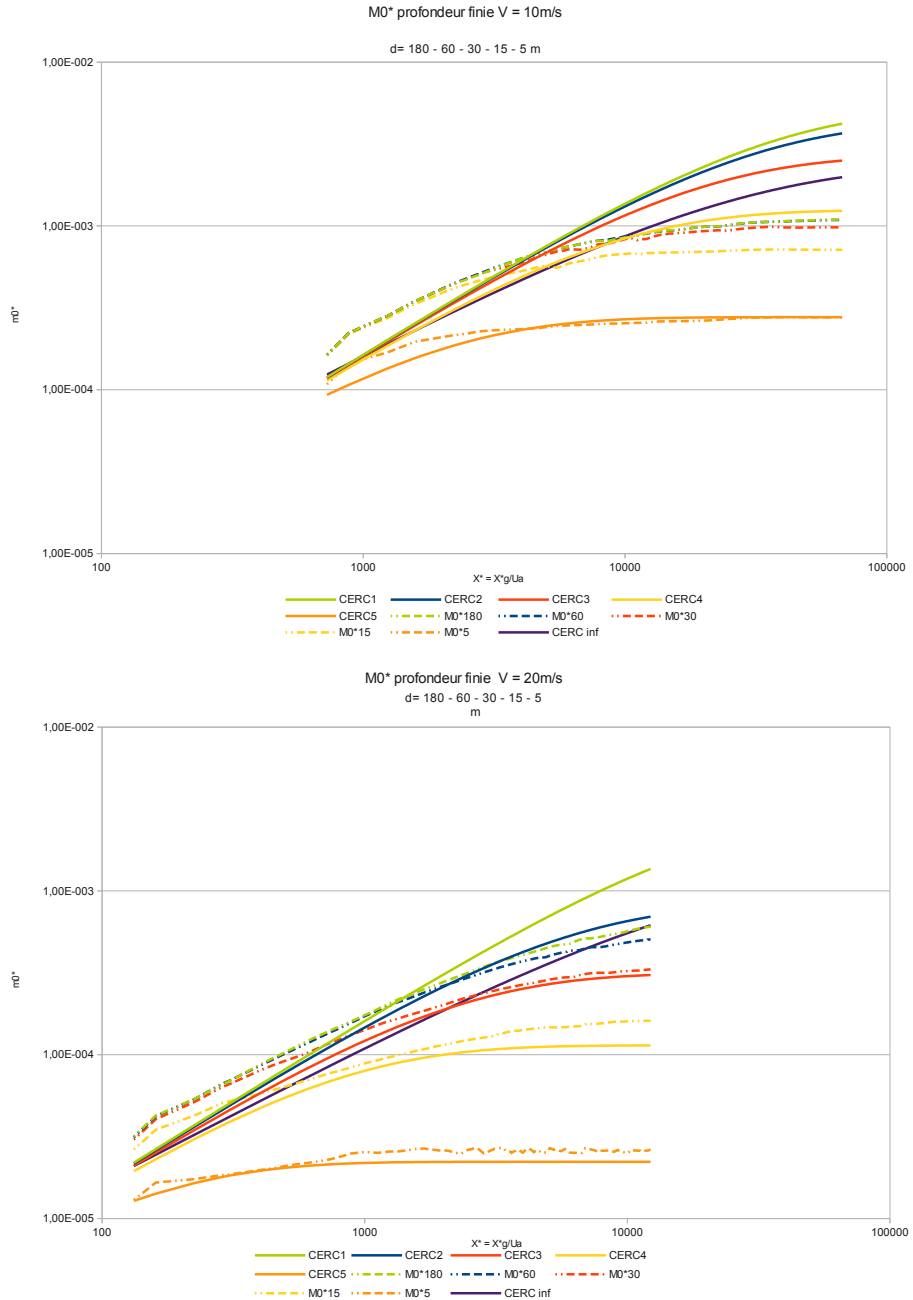


Figure 3.22: Comparaison of normalized Variance $M0^*$ for $U_{10} = 10 \text{ m/s}$ (high) and 20 m/s (bottom) for different depths : 5, 15, 30, 60, 180 m

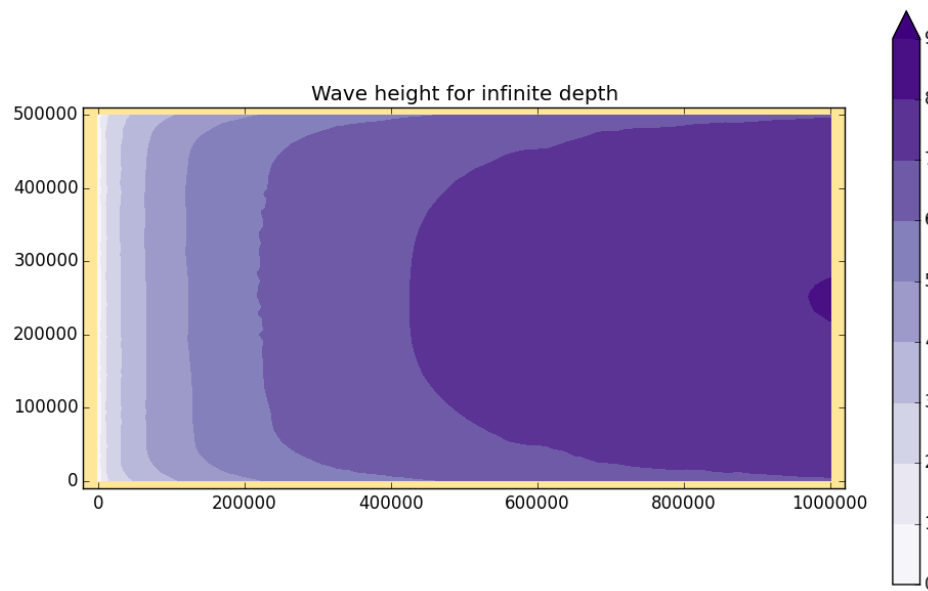


Figure 3.23: wave heighth for infinite depth

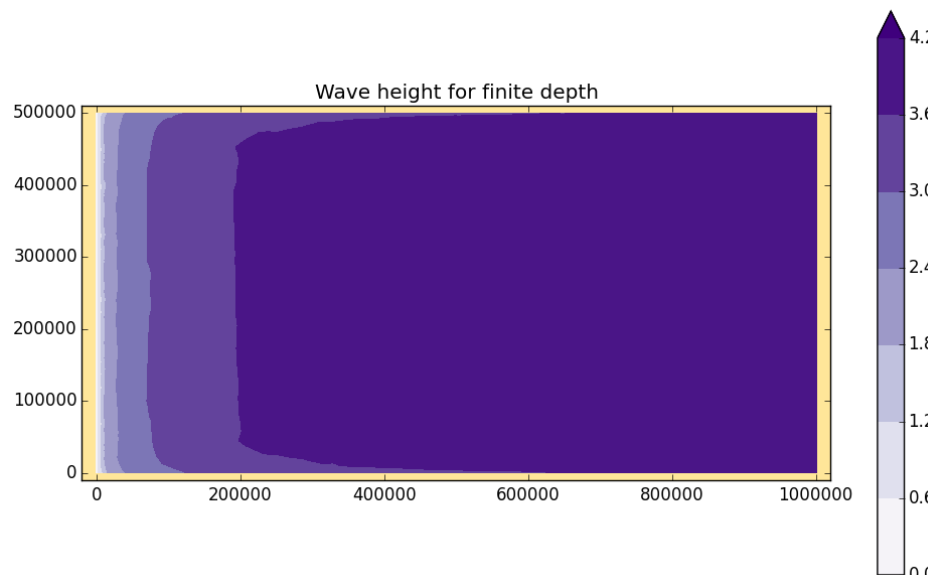


Figure 3.24: wave heighth for finite depth

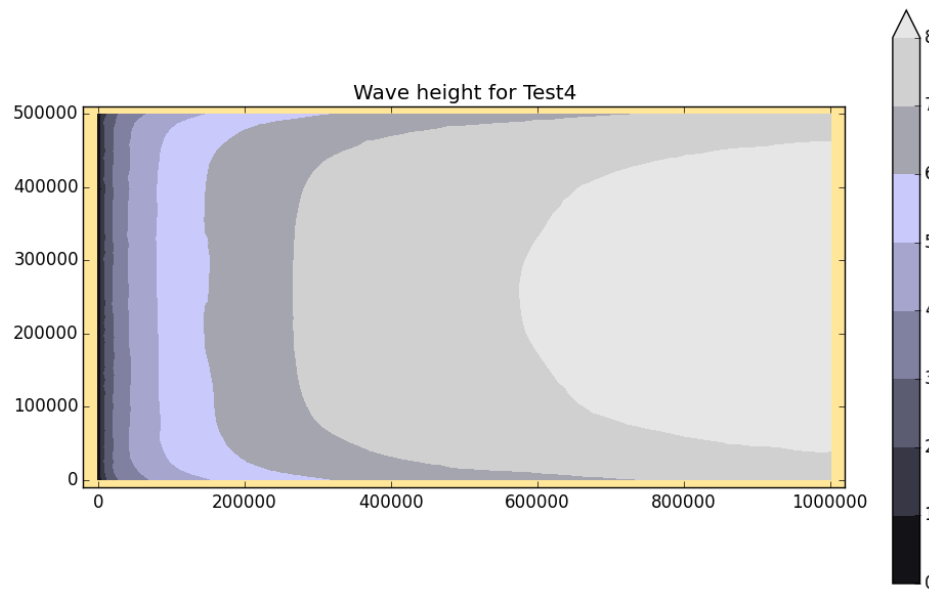


Figure 3.25: wave heighth for test4

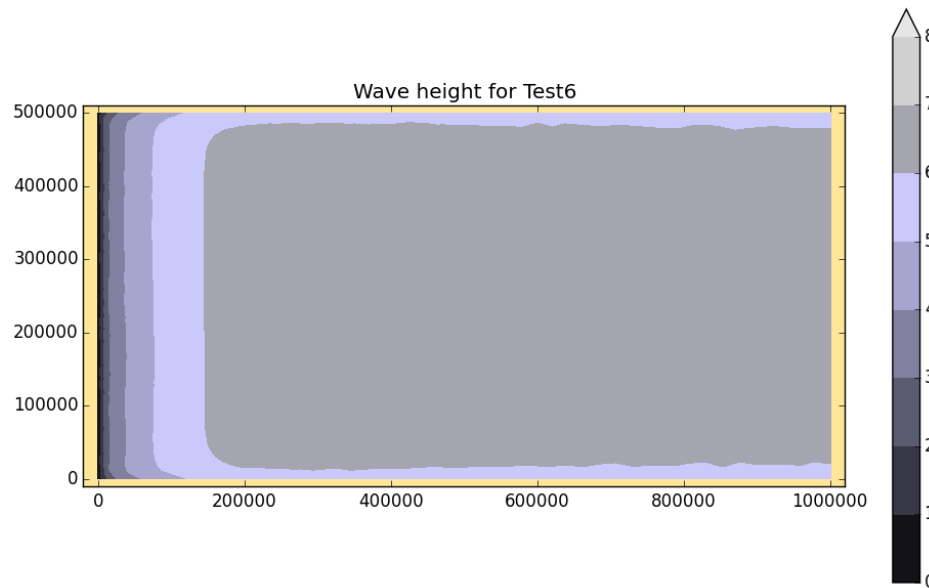


Figure 3.26: wave heighth for test6

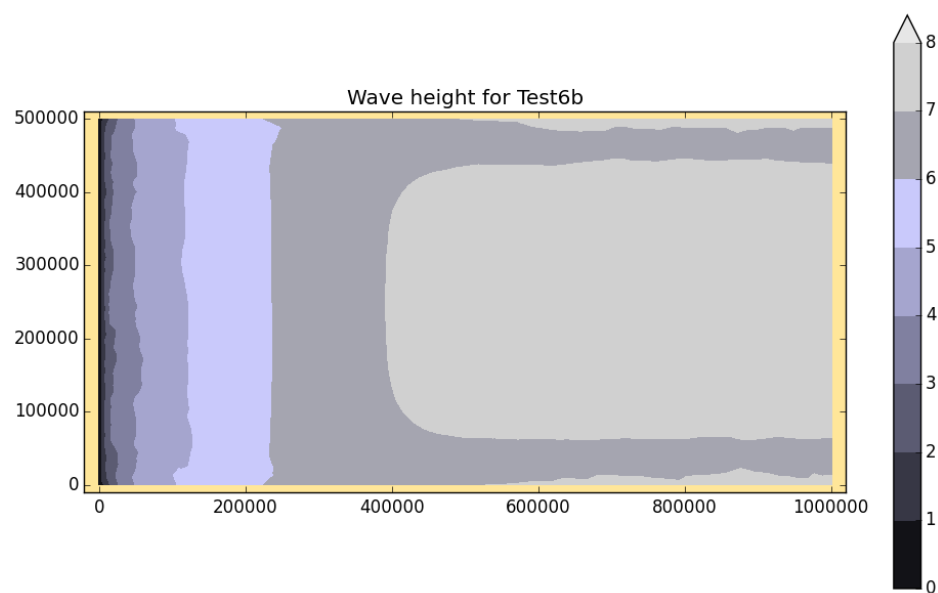


Figure 3.27: wave heighth for test6b

3.10 Opposing current

3.10.1 Purpose

The goal of this test-case is to check the behaviour of TOMAWAC in presence of a strong opposing current. When water meets the strong adverse current, with a velocity that approaches the wave group velocity, waves are blocked. Without any option for strong current, the amplitud of waves is overestimated.

3.10.2 Description of the problem

We present here the simulation of the test case of Lai [16]. We present two different options that prevent from overestimation.

Option 1 : consider an equilibrium range spectrum (in the presence of ambient flow) applied as an upper limit for the spectrum Hedges et al ([11])

Option 2 : add a dissipative term on the right-hand side of the action balance equation [8]

For more details on formulations, one can refer to Tomawac documentation, paragraphs 4.2.3.8.1 and 4.2.3.8.2.

3.10.3 Reference

The flume experiment of Lai et al [16] investigates the transformation of the wave spectrum on a strong negative current gradient in a flume of 8 m length and 0.75 m depth. An opposing current flow is induced along the flume according to figure 3.28

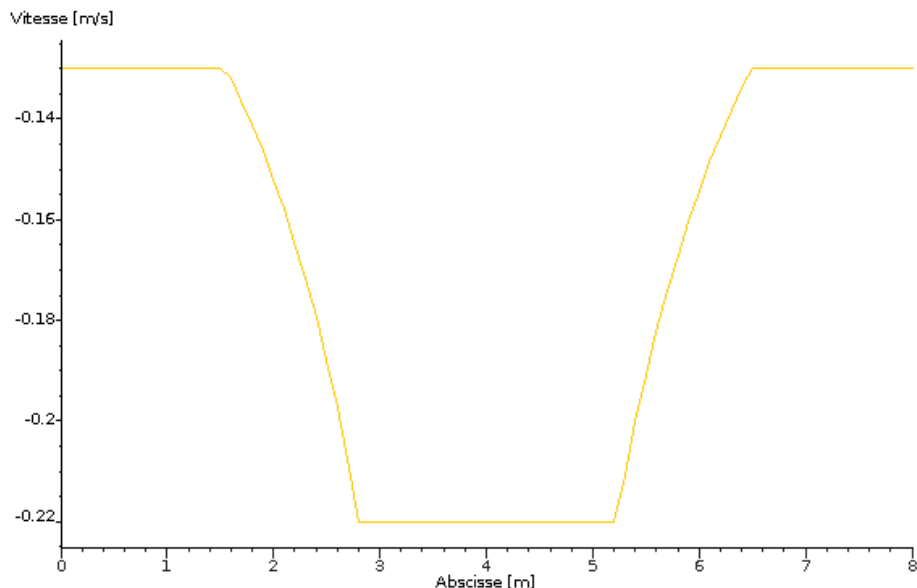


Figure 3.28: courant of the test case

3.10.4 Physical parameters

Concerning the modelling of the opposing current with the first option the Phillips's constant in the Pierson-Moskowitz spectrum is equal to 0.0081. For the second option of this modelling, the dissipation coefficient is equal to 0.65, and saturation threshold value is taken to $1.75 \cdot 10^{-3}$. The white-capping dissipation is the model of Westhuysen 2008. Non linear transferts between frequencies are calculated by the DIA method.

3.10.5 Geometry and Mesh

The bathymetry is as described on figure 3.29.

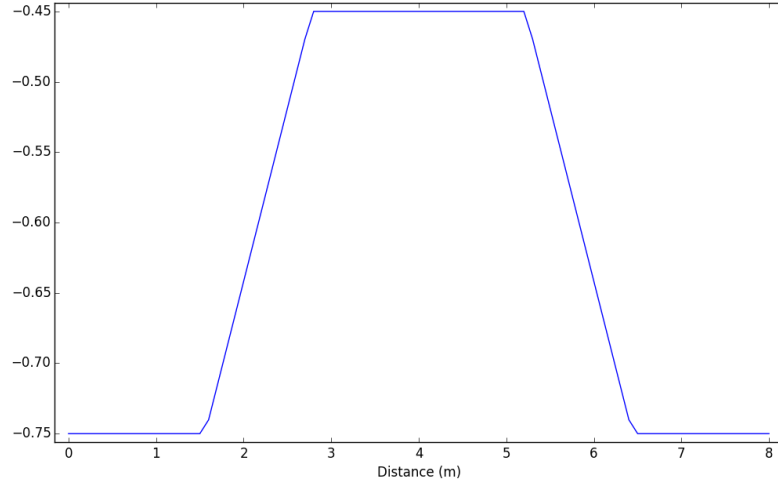


Figure 3.29: bathymetry of the test case

The mesh is made of 1701 nodes and 3200 triangles and is shown Figure 3.30.

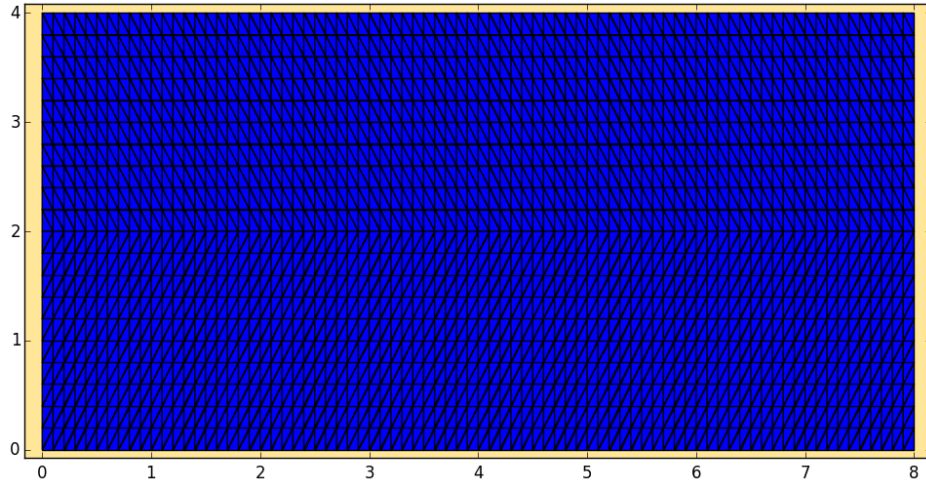


Figure 3.30: Mesh of the domain

3.10.6 Initial and Boundary Conditions

For both conditions, we take a Jonswap spectrum with a 1.9 cm significant wave height, a peak frequency of 2.2. The angular distribution function follows a $\cos^2 \theta$ distribution with an angular spreading of 65 and a mean direction of 90.

3.10.7 Numerical parameters

Time duration is 400 s, time step is equal to 0.1 s, the spectro-angular mesh has 72 angles and 36 frequencies spread on a geometric progression common ratio 1.1 with a minimum of 0.25. The option for wave growth limiter is following the Hersbach et Janssen (1999) parameterisation.

3.10.8 Results

We show the results obtained Figure 3.31. The two options are efficient to reduce the wave height overestimation and lead to a solution closer to measurements. This shows the interest of including these options in the case of a strong opposing current.

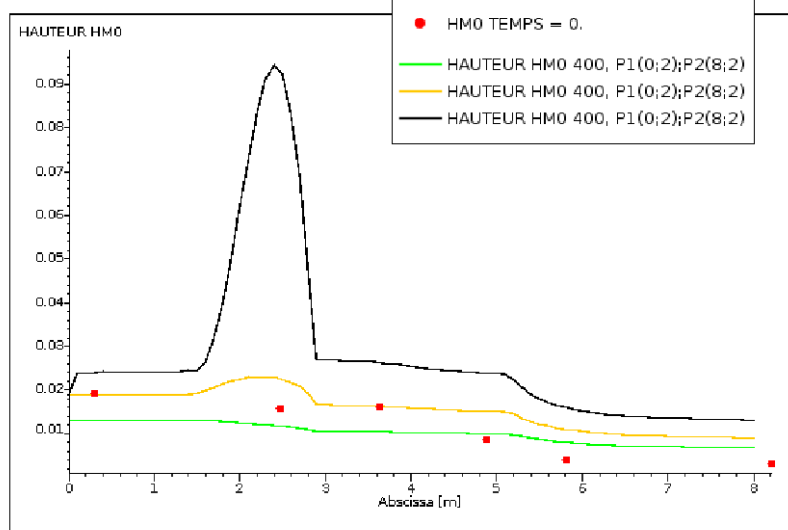


Figure 3.31: Height comparison without wave blocking and with the two options.

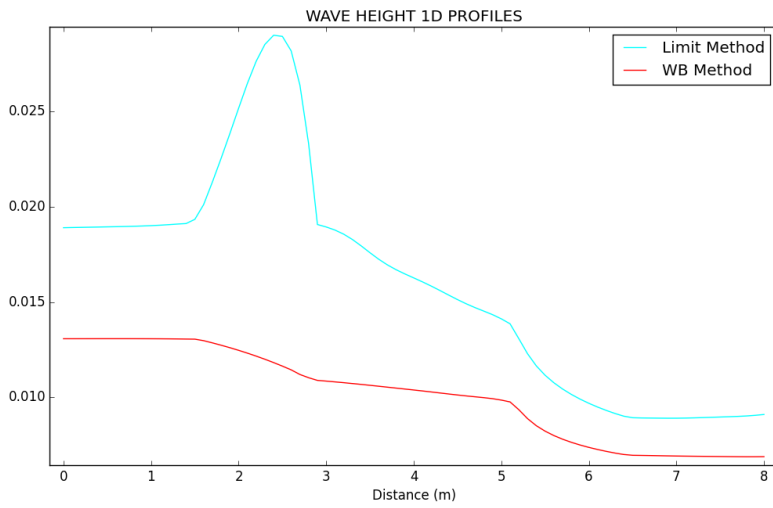


Figure 3.32: Height comparison with the two options for the last validation.

Test number	Case ID	Type	Period (sec)	Height (cm)	α	γ	σ_m (deg)
(a) Initial Series							
1	M1	Mono	1.30	5.50	—	—	—
2	N1	Spec	1.30	7.75	0.01440	2	10
3	B1	Spec	1.30	7.75	0.01440	2	30
4	N2	Spec	1.30	7.75	0.00440	20	10
5	B2	Spec	1.30	7.75	0.00440	20	30

Table 3.2: Test conditions for shoal test series, Vincent and Briggs experiments

3.11 Shoal : Submerged elliptical mound

3.11.1 Purpose

The goal of this test-case is to check the behaviour of TOMAWAC in presence of refraction, shoaling and diffraction effects over a shoal.

A shoal causes a concentration area of wave just behind it, what makes fail numerical models of refraction based on the radius theory. This test-case allows to verify simulations from TOMAWAC for refraction, shoaling and diffraction processes.

3.11.2 Reference experiments

The references of this test-case are the experiments of [27]. They worked on the refraction and the diffraction of irregular waves over a mound using a directional spectral wave generator and they measured the wave's height.

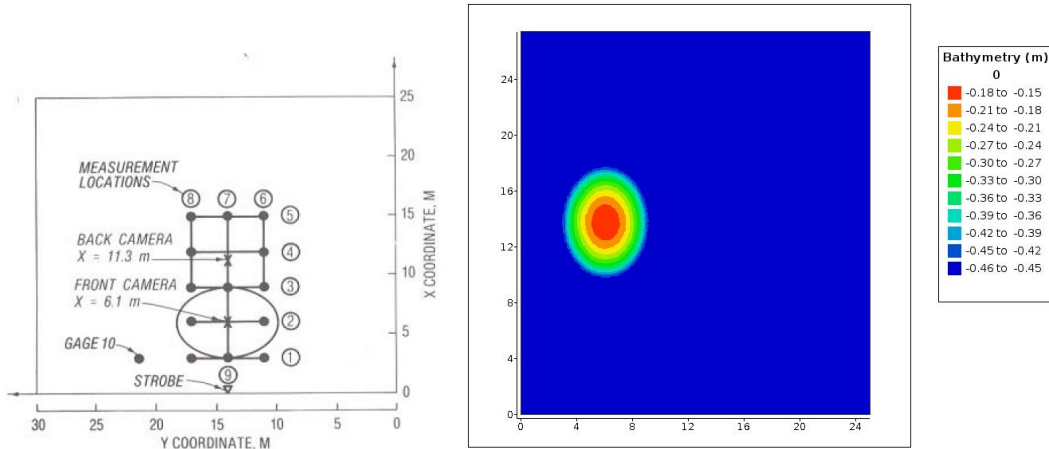


Figure 3.33: Set up of Vincent and Briggs experiments

Different irregular wave conditions were tested, varying the narrowness and the directional spread of the spectrum. They used a TMA shallow-water spectrum (Bouws et al. 1985) and a wrapped normal spreading function which can be close to a Mitsuyasu directional spreading function.

In this benchmark, only one type of wave condition is tested for the diffraction effects, the N1 one. But B1, B2, N1 and N2 are tested to evaluate the refraction and the shoaling.

3.11.3 Test-case description

The case is about spectral wave propagation on a submerged elliptical mound. The study will compare the spectral significant wave heights given by TOMAWAC simulations with measurements from [27]'s experiments.

Geometry of the domain and bathymetry

Bassin	dimension :	27.43 m * 18.3 m
	depth constant outside the shoal :	0.4572m
Elliptical shoal	major radius :	3.96m
	minor radius :	3.05m
	maximum height :	0.305m
	coordinates of the center :	(6.10,13.72)

The elliptical shoal is defined by :

$$a = \left(\frac{x}{3.96} \right) + \left(\frac{y}{3.05} \right) \quad \begin{cases} \text{if } a \geq 1, Zf = -0.4572 \\ \text{if } a < 1, Zf = -0.9144 + 0.762\sqrt{1 - 0.64a} \end{cases}$$

Meshes

Spatial discretization

Three meshes are used for the simulation :

- finer : Element size at the shoal 0.2 m $\Delta x/\lambda = 0.09$
- medium : Element size at the shoal 0.4 m $\Delta x/\lambda = 0.18$
- coarser : Element size at the shoal 0.8 m $\Delta x/\lambda = 0.35$

Where λ is the wavelength.

Spectro-angular discretization

- 22 frequencies (0.35 - 2.85 Hz)
- logarithmic scale ($\Delta f/f = 0.1$)
- 36 directions

Initial and Boundary conditions

The domain is initially at rest. The incident wave conditions are the following:

- the incident wave conditions are imposed at the boundary representative of the wave generator. All the others are absorbing boundaries.
- Frequency spectrum : TMA shallow water spectrum

$$S(f, \theta) = E(f) * D(\theta)$$

$$E(f) = \frac{\alpha g^2}{(2\pi)^4} f^{-5} \exp(-1.25(\frac{f_p}{f})^4) * \gamma^{\exp(-0.5(\frac{f-f_p}{\sigma f_p})^2)} * \phi(f, d)$$

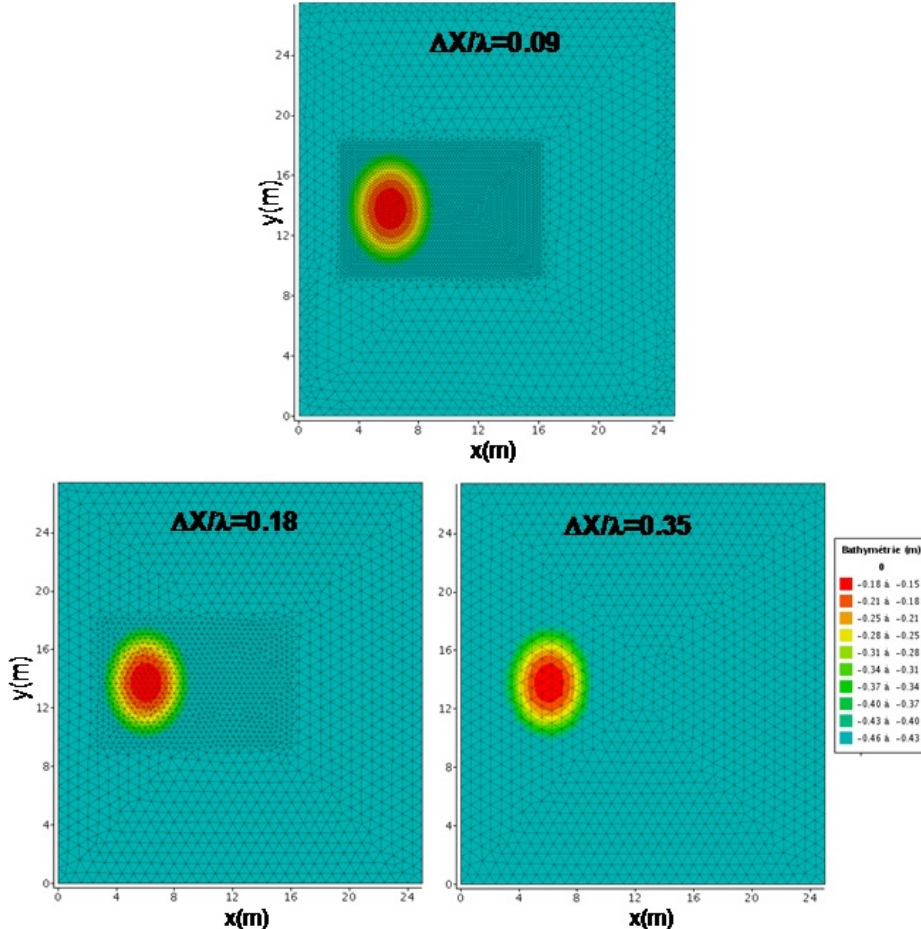


Figure 3.34: The different meshes used

- Directional spreading function: gaussian type

$$D(\theta) = \frac{1}{\sqrt{2\pi}\sigma_m} \exp\left[-\frac{(\theta - \theta_m)^2}{2\sigma_m^2}\right]$$

Where :

- α : Phillips constant
- f_p : peak frequency ($f_p = 0.769$ Hz)
- γ : peak factor
- $\sigma = \begin{cases} 0.07 & \text{if } f < f_p \\ 0.09 & \text{if } f > f_p \end{cases}$
- $\phi(f, d)$ is a factor which allows the consideration of depth effects:

$$\phi(f, d) = \begin{cases} 0.5w_p^2 & \text{if } w_d \leq 1 \\ 1 - 0.5(2 - w_d)^2 & \text{if } 1 < w_d < 2 \\ 1 & \text{if } 2 \leq w_d \end{cases}$$

with $w_d = 2\pi f(d/g)^{1/2}$

- θ_m : mean wave direction at frequency f
- σ_m : directional spreading parameter

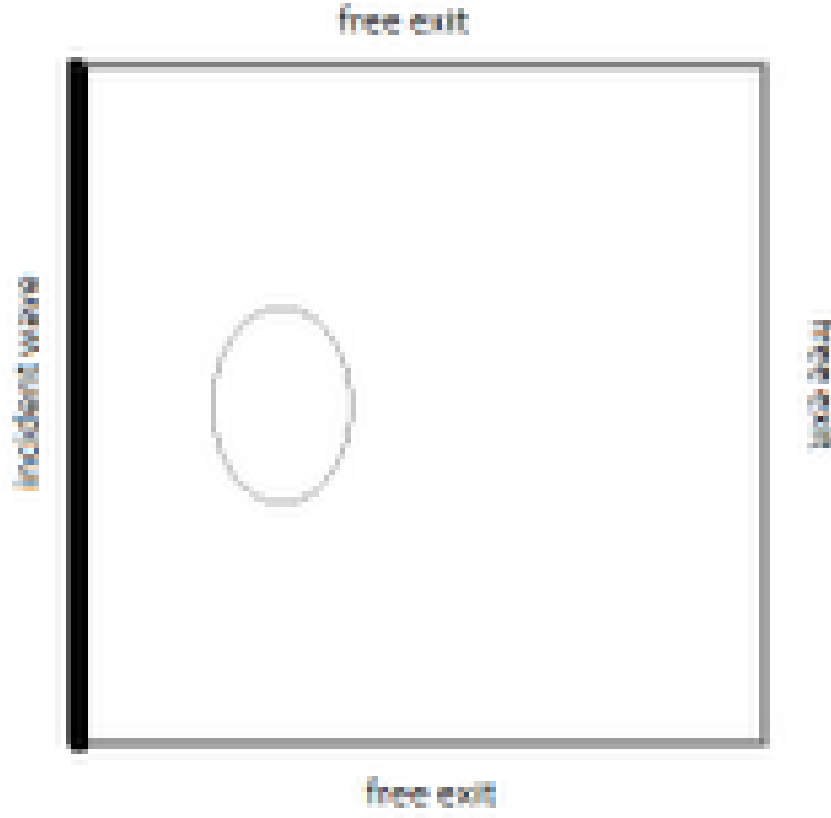


Figure 3.35: The boundary conditions

3.11.4 Numerical parameters

- time steps :
 1. $\Delta x/\lambda = 0.09 \rightarrow \Delta t = 0.005$
 2. $\Delta x/\lambda = 0.18 \rightarrow \Delta t = 0.025$
 3. $\Delta x/\lambda = 0.35 \rightarrow \Delta t = 0.1$
- CPU times :

$\Delta x/\lambda = 0.09$	$\Delta x/\lambda = 0.18$	$\Delta x/\lambda = 0.35$	
B1	-	1569 s	209 s
B2	-	1387 s	211 s
N2	-	1534 s	239 s
N1	4027 s	1359 s	229 s

3.11.5 TOMAWAC Results

At first, simulations without diffraction effects are done in order to validate the propagation and refraction of the wave over this complex bathymetry. To compare the simulation results and

the measurements of [27], the significant wave heights have been normalized by the incident significant wave height.

- B1 and B2 tests (wide directional spreading):

A good matching can be seen in these tests (see Figure 3.36). After drawing the iso-wave-height compared to the [27]’s measurements, the wave concentration zone is well represented. The amplification factor goes over 1.3 for B1 and 1.4 for B2. As in measurements, this amplification factor is a bit higher for B2 case (higher peak factor) than for B1 case. But simulation factors are a little bit higher than those measured.

Moreover, the computations of normalized wave height along the transect 4 match quite well with the measurements (not shown here).

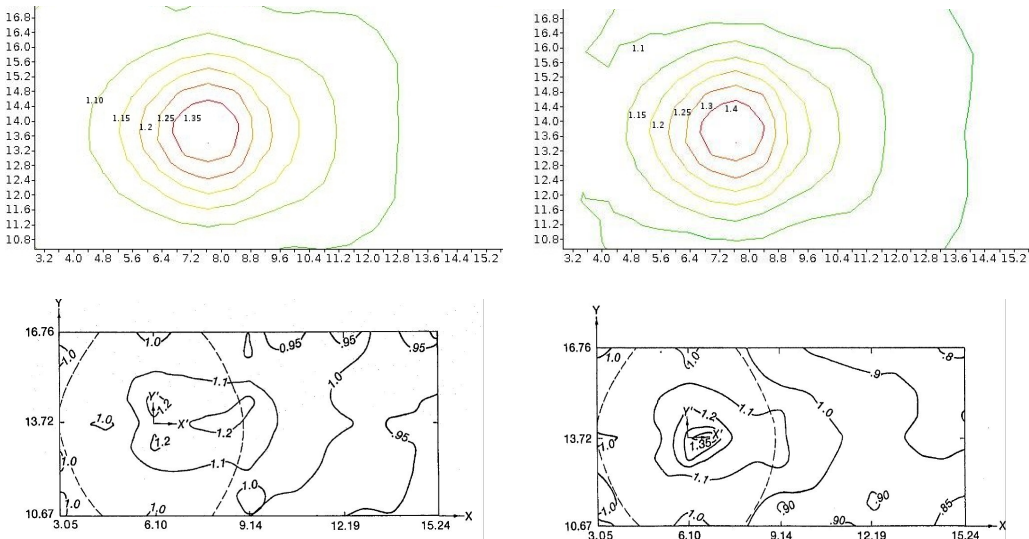


Figure 3.36: Comparaison of normalized significant wave height iso-lines for the B1 (left) and B2 (right) tests with the measurements from Vincent and Briggs (coarser mesh).

- N1 and N2 tests (narrow directional spreading):

These tests are not as good as the B ones because only one area of big wave heights is shown while two are highlighted in measurements. Also the amplification factors are bigger than those measured. It can be explained by the lack of representation of the diffraction effects. But again, the results along the transect 4 show a coherence of the simulation and the measurements. (see Figure 3.37 for N2, and Figure 3.39 for N1).

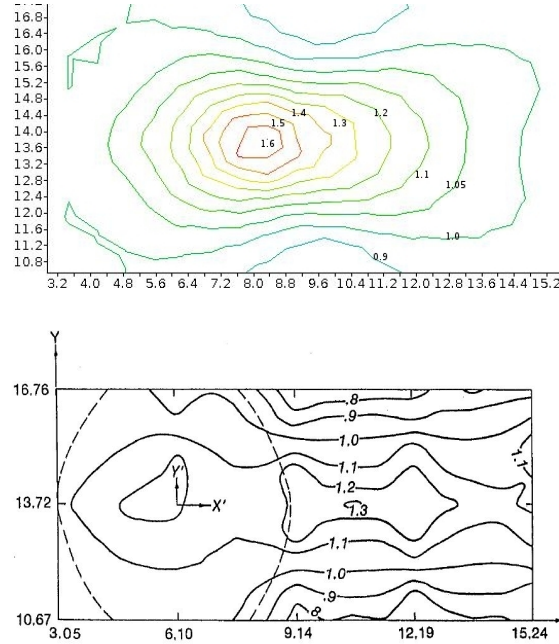


Figure 3.37: Comparaison between normalised iso-line TOMAWAC results and Vincent measurements for the case N2 (coarser mesh).

Subsequently, the computation will include diffraction effects. The diffraction coefficient K_d is defined by the ratio of the spectral significant wave height to the spectral significant incident wave height, $K_d = \frac{H_{m0}}{H_{m0_inc}}$.

Parametrical tests have shown the influence of two non-dimensional parameters: the ratio of the mesh size over the wavelength ($\Delta x/\lambda$) and the current number. The courant number Cr is: $Cr = \frac{C_g(f_p)\Delta t}{\Delta x}$.

where $C_g(f_p)$ is the group velocity associated to the sea-state peak frequency, Δt the simulation time step and Δx the size of the smallest element of the mesh.

The diffraction coefficients obtained during the simulations (changing Cr and $\Delta x/\lambda$) are compared with measurements [27] and the iso- K_d curves resulting from TOMAWAC simulations are superposed with the ones measured by Vincent and Briggs. (see Figure 3.40).

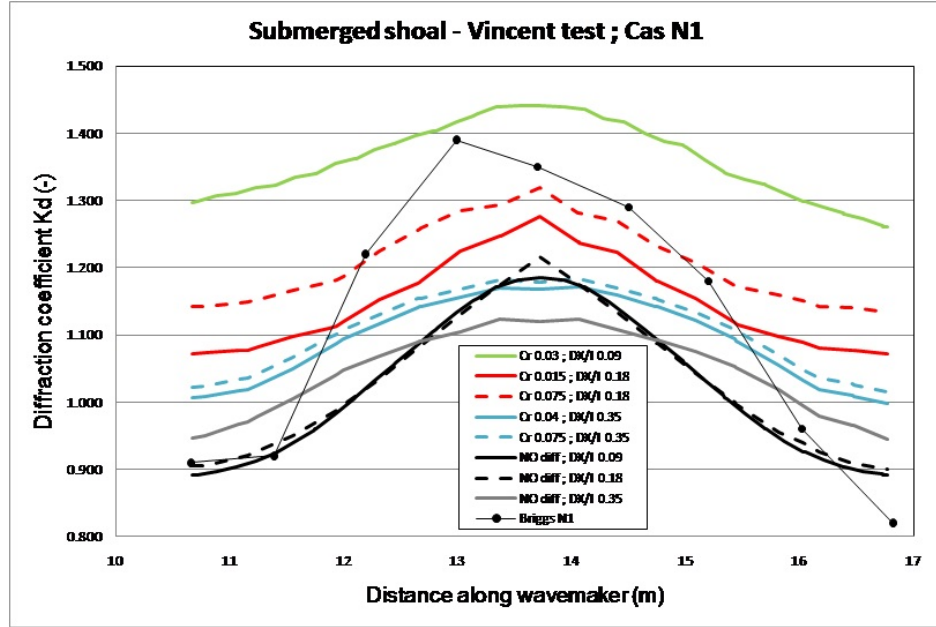


Figure 3.38: Comparaison between TOMAWAC results and Vincent measurements: measured and simulated values of the diffraction coefficient along the transect 4 (see Table 3.2) of the model.

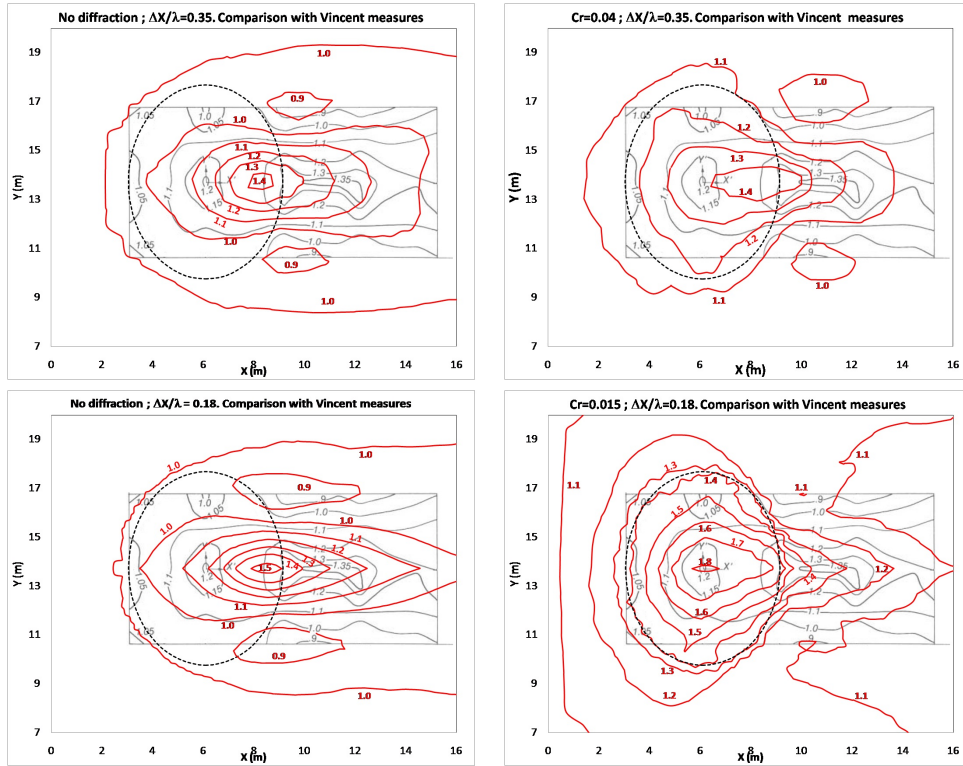


Figure 3.39: Comparaison between TOMAWAC results and Vincent measurements: measured and simulated iso- K_d curves over and behind the mound for the case N1

As one can see in these two graphs (Figures 3.38 & 3.39), the diffraction effects over the shoal are not well simulated by TOMAWAC due to a large build-up of energy. Indeed the larger Cr

is and the finer the mesh is, the larger the numerical and the energy build-up are. Moreover with the coarser mesh ($\Delta x/\lambda = 0.35$) TOMAWAC is not able to capture the diffraction effects generated by the submerged shoal. In the Figure 3.39, the simulation's curves are too flattened and the curves that have the shape closest to the measurements are the No diffraction ones. Also in the iso-Kd graph, the curves do not superimpose well when diffraction is taken into account, but for the case with only propagation and refraction the correspondance is correct. Indeed, we can see that the iso-line shapes are closest to the measured ones.

Mainly, the build-up and the numerical noise are generated when a high resolution of the mesh is used and they are due to the meshfree algorithm (used to compute second derivatives during simulation). In order to improve the simulation of the diffraction effects, a spatial filter is built to limit the energy build-up. The effect of this filter can be seen on the diffraction coefficient Kd (see Figure 3.40). The noise and the energy build-up effects are reduced but it does not improve the quality of the results significantly.

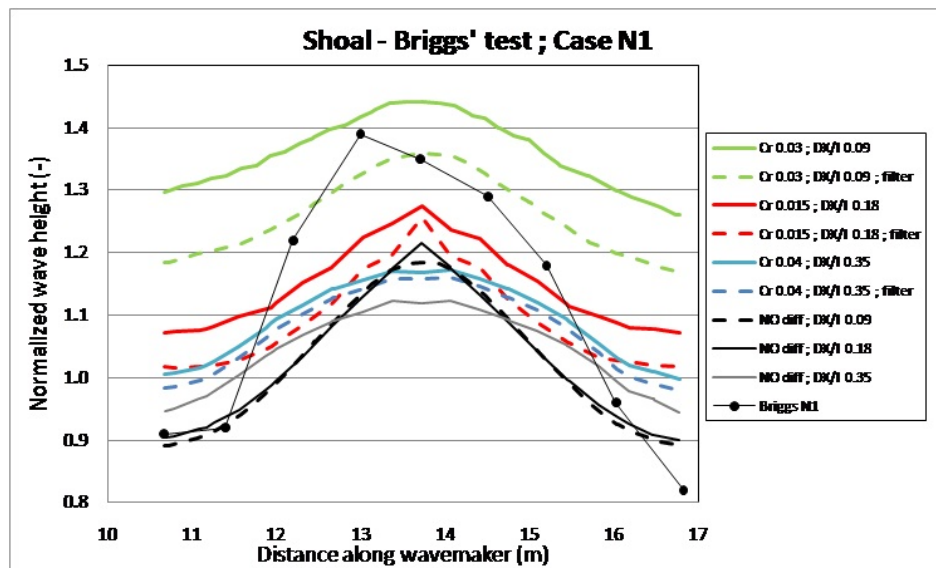


Figure 3.40: Comparaison between TOMAWAC results and Vincent measurements: measured and simulated values using a filter of the diffraction coefficient along the transect 4 of the model

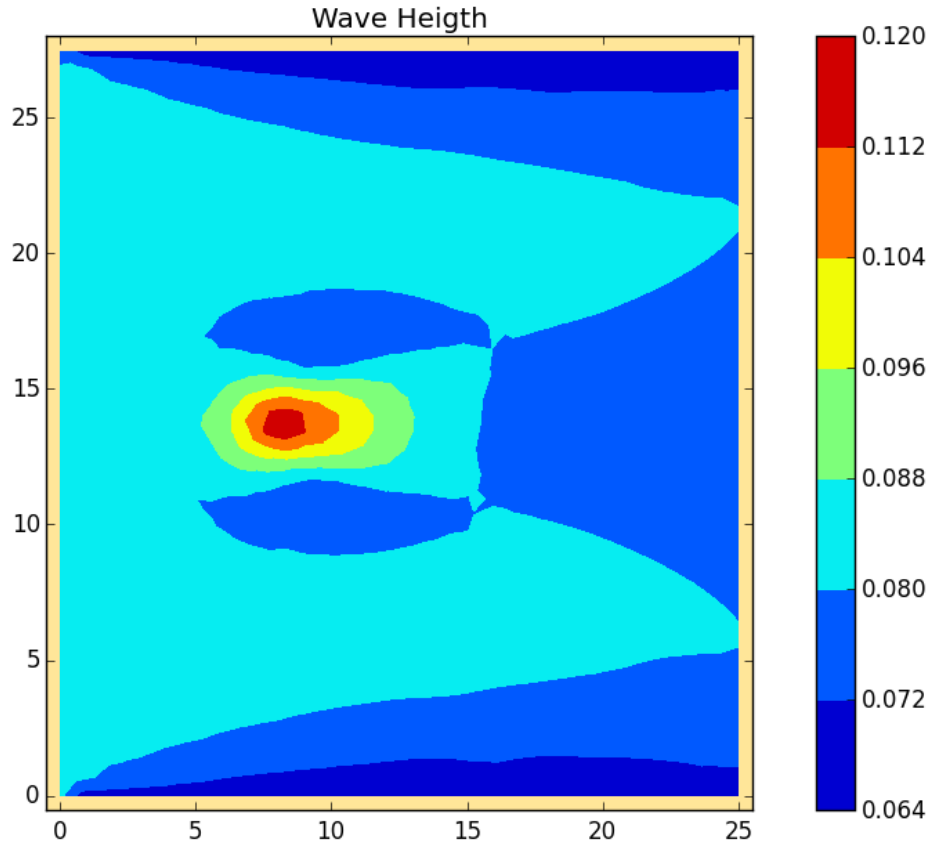


Figure 3.41: WAVE HEIGHT HM0 for the last calculation.

3.11.6 Conclusion

This benchmark test allows to compare simulations from TOMAWAC and experimental results. It follows that TOMAWAC provides a correct simulation of the propagation, shoaling and the refraction but the diffraction effects are limited and not really well represented. In order to improve the results, a smoothing filter can be applied on the spatial domain.

3.12 Turning wind

3.12.1 Purpose

This test case shows how Tomawac calculate the spectrum when there is a wind that is turning. It illustrates the phenomena of white capping and quadruplet interactions. This document is a short translation of the french 'doc' version. One can find more details in *turning_wind/doc/turningwind.doc*

3.12.2 Description of the problem

The domain is homogeneous, The depth is infinite, the wind given at 10m is homogeneous propagation step is inhibited and no boundary condition are given. So the domain of computation can be reduced to a few points as the solution is homogeneous and finally we focus on only one of them. The domain is finally very simple (see Figure 3.42)

3.12.3 Physical parameters

The modulus of the wind is constant, equal to 20 m/s. Initially the direction is set to 90 degrees, (which means that U_Y is null). This is maintained till the peak frequency reaches the double of its equilibrium value (peak frequency of Pierson-Moskowitz). This occurs after 28800 s (8h), at this time we change the direction of wind for 30 degrees (a rotation of 60 degrees). All the values of the wind are read in a file called *wind.slf*.

3.12.4 Geometry and Mesh

The domain is a square of 2 km. The mesh is very simple as there are 5 nodes and 4 triangles. That also means that this case can not be run in parallel.

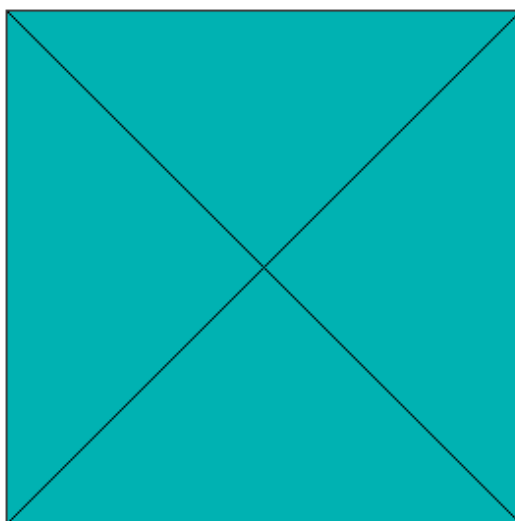


Figure 3.42: Mesh of the domain

3.12.5 Initial and Boundary Conditions

Initial conditions are imposed homogeneous on the domain with the option 4, with a Phillips constant of 0.024 an initial peak frequency of 0.3 Hz and an initial peak factor of 1. The initial directionnal spread is set to one and the initial main direction to 90 degrees (like the wind). Those value has been set to be identical to the Vledder study [24]

Nothing is imposed at the boundaries.

3.12.6 Numerical parameters

Time duration is set to 115200s (32h), time step is equal to 900s, the spectro-angular mesh has 12 angles and 26 frequencies spread on a geometric progression common ratio 1.1 with a minimum of 0.04177248.

3.12.7 Results

We present here the results only for the rotation of 60 degrees as it is the effective rotation that is done in the case. Initially there were 2 more rotations one of 90 degrees and one of 30 degrees. The results for those rotations are described in [17].

At the moment when the direction changes the established swell is going to interact with the wave induced by the new direction of wind. Three phenomena occur in that process.

- Wind contribution to the energy that will raise the new wave,
- Attenuation of the swell part of the spectrum,
- Non linear interactions between swell and wind sea.

The results of Tomawac are compared to simulations made by two different codes. EXACT-NL and WAM-cycle 3 (see [24]). Figure 3.43 shows that there are good agreements of Tomawac results compared to other simulations. One can note that the spectrum tail factor can be sensitive. During the first 4 hours a factor 4 is better but after that time a factor 5 is better.

Let us remark that those are old results and a new simulation with new linear terms might give better results.

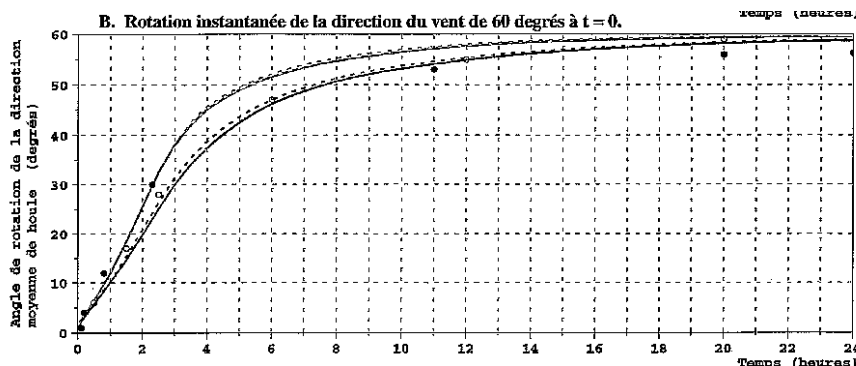


Figure 3.43: Comparison of direction of wave with time after a direction change of 60 degree at $t=0$. Simulations are made for different spectrum tail factor and different initial spectrum

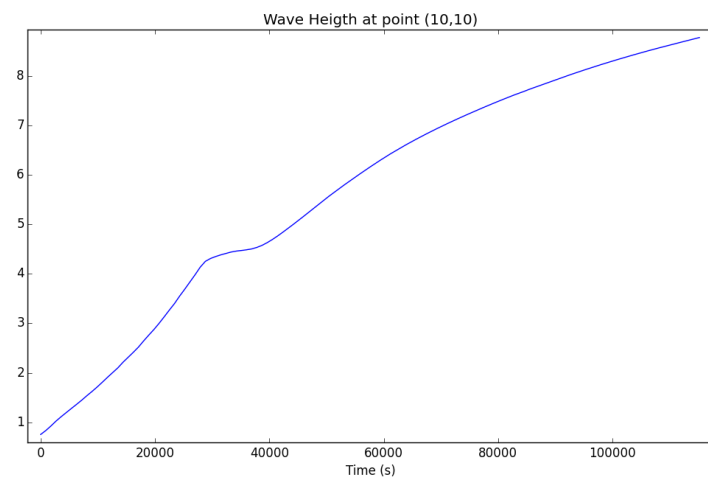


Figure 3.44: WAVE HEIGHT HM0 when winds changes for the last calculation.

3.13 Whirl current

3.13.1 Purpose

This test case should make it possible to check that the effects of refraction by the current are properly taken into account by Tomawac 7.0. The distortion of a wave spectrum as it reaches a whirl current zone like those observed along the Norwegian coasts [18]

3.13.2 Description of the problem

This test case is derived from the Mathiesen's results [18]. Equivalent results can be found in [12] and [29]. The spatial domain is a 80 km-sided square (see Figure 3.45). A circular, origin-centered whirl current is considered ; it is modelled as follows. Its tangential velocity is zero at the origin and linearly increases up to $r = r_l$ as per :

$$u(r) = u_l \frac{r}{r_l} \text{ for } r \leq r_l \leq r_0$$

Then, that velocity follows a Gaussian profile:

$$u(r) = u_{max} \exp \left(- \left(\frac{r - r_0}{br_0} \right)^2 \right) \text{ for } r > r_l$$

Both continuity and derivability for u lead to:

$$\frac{r_l}{r_0} = \frac{1 + \sqrt{1 - 2b^2}}{2}$$

$$\frac{u_l}{u_{max}} = \exp \left(- \left(\frac{r_l - r_0}{br_0} \right)^2 \right)$$

The following values were adopted in the computations: $u_{max} = 1m/s$, $r_0 = 10km$ and $b = 0.3$. The model as developed by Mathiesen is a refraction model that computes the orthogonal waves through a conventional ray method. The results it provides for the 0.1 Hz frequency are displayed on Figure 3.46. Many orthogonal crossings can be observed.

3.13.3 Initial and Boundary Conditions

That method of rays can be implemented either forwards (as on Figure 3.46), or backwards, then knowing the arrival point of an orthogonal, it provides the starting point. A whole wave spectrum can be reconstructed by multiplying the computations of this kind. The incident spectrum as prescribed by [18] is as follows :

$$S(f, \theta) = S(f)D(f, \theta)$$

In that expression $S(f)$ is a frequency spectrum of the classical Jonswap type, where the peak frequency f_p is set to 0.1 Hz. $D(f, \theta)$ is a Gaussian distribution:

$$D(f, \theta) = \frac{\exp \left(-\frac{(\theta - \theta_m)^2}{2\sigma_0^2} \right)}{\sqrt{2\pi}\sigma_0}$$

θ_m is the mean direction of the incident waves (here $\theta_m = 0$) and σ_0 is given by the following relationship.

$$\sigma_0 = \sigma_{0p} \left(\frac{f}{f_p} \right)^{-2.03} \text{ if } f < f_p$$

$$\sigma_0 = \sigma_{0p} \left(\frac{f}{f_p} \right)^{1.04} \text{ if } f \geq f_p$$

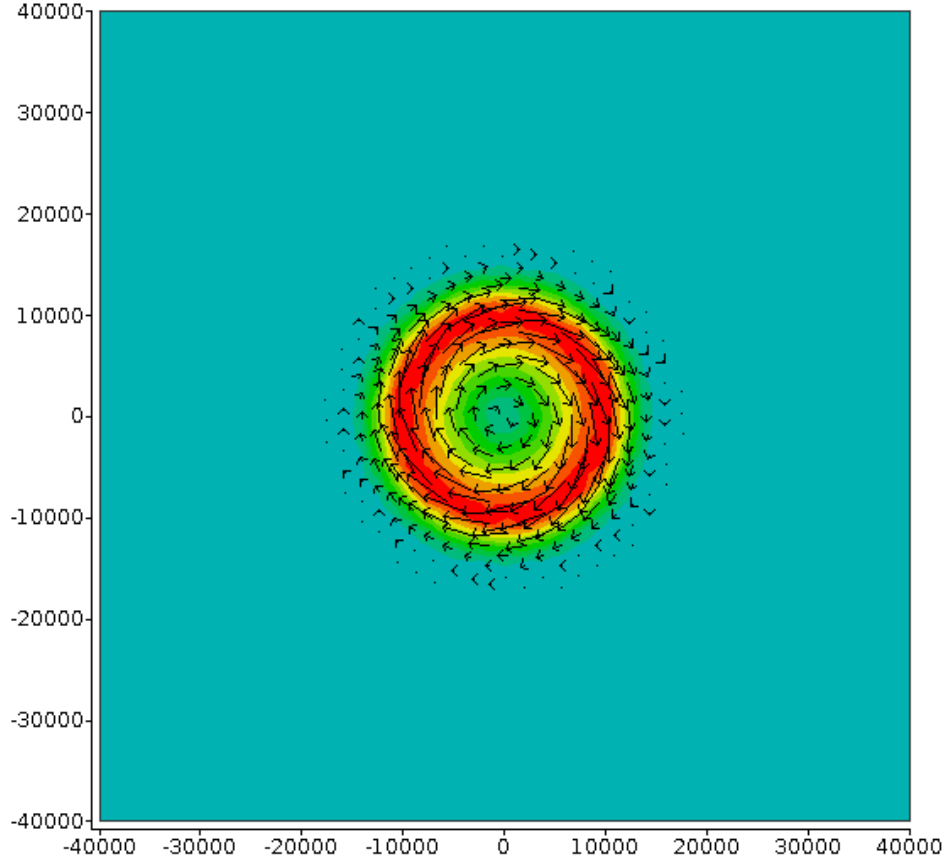


Figure 3.45: whirl current

where σ_{0p} , the directional spread at the peak, is 25 in our case. This spectrum is imposed on the East South and West boundaries while the North boundary is free.

The initial spectrum is null.

3.13.4 Geometry and Mesh

The mesh is made of 1876 nodes and 3590 triangles and is shown Figure 3.47

3.13.5 Numerical parameters

Time duration is 60000 s, time step is equal to 1200 s, the spectro-angular mesh has 48 angles and 25 frequencies spread on a geometric progression common ratio 1.1 with a minimum of 0.04177248.

3.13.6 Results

On figure 3.48, we present the amplification factor of the height due to the current. We can notice two different zones at the center of the domain where there is a strong modification of the height. One zone where the height is raising (till 35%) when the swell is opposed to the current, and one zone where the height is decreasing (till 20%) where swell and current are in the same direction. On the other parts of the domain, modifications are less than 5%. Those results are coherent with the ray calculus presented on Figure 3.46 since on the two zones we denote orthogonal crossing.

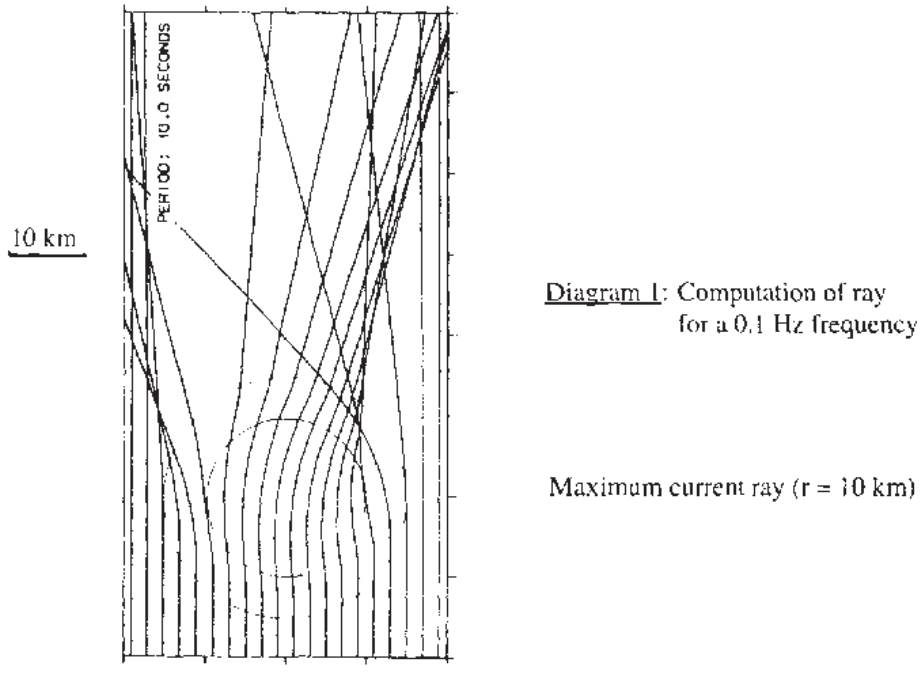


Figure 3.46: Computation of rays

In his paper, Mathiesen [18] defines 8 points shown on Figure 3.48. On these points he gives the energy angular spread at 0.1 Hz (frequency peak of the incident spectrum). We compare this spread to the one obtained by Tomawac on Figure 3.49. We can denote that the results are very closed to Mathiesen results especially on points 4 and 7. Notice that Mathiesen took an angular discretisation of 2.5 when our is of 7.5.

3.13.7 Conclusion

This test case showed on a realistic case of refraction of current that Tomawac gives suitable results compared to fine results.

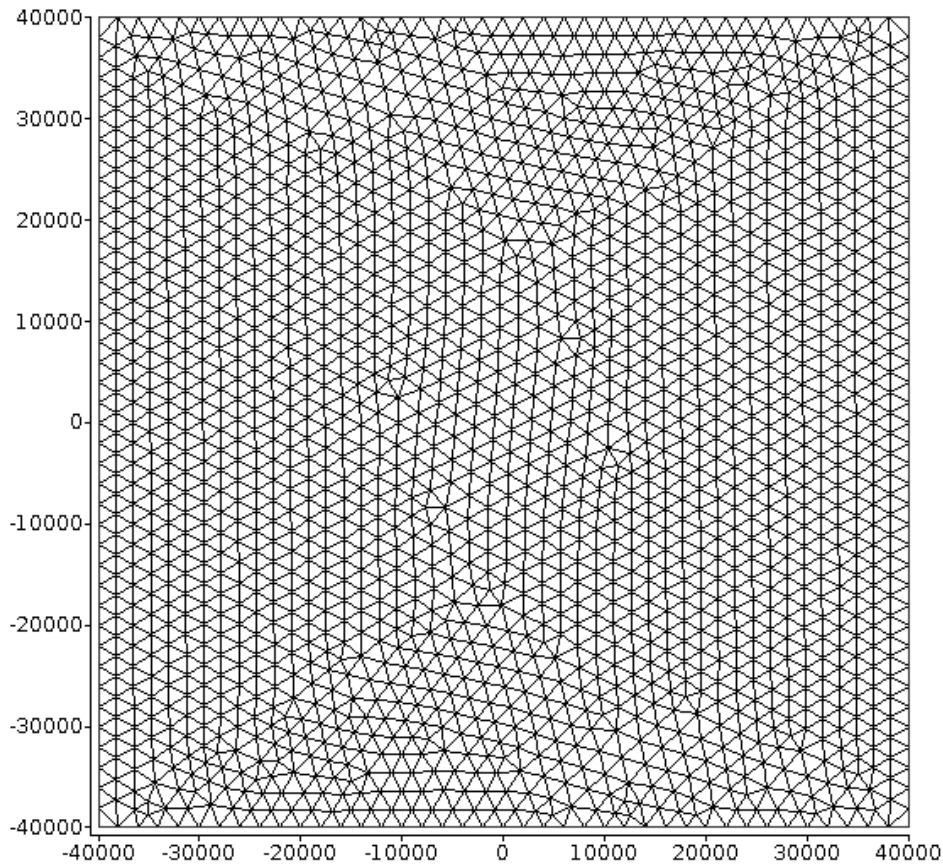


Figure 3.47: Mesh of the domain

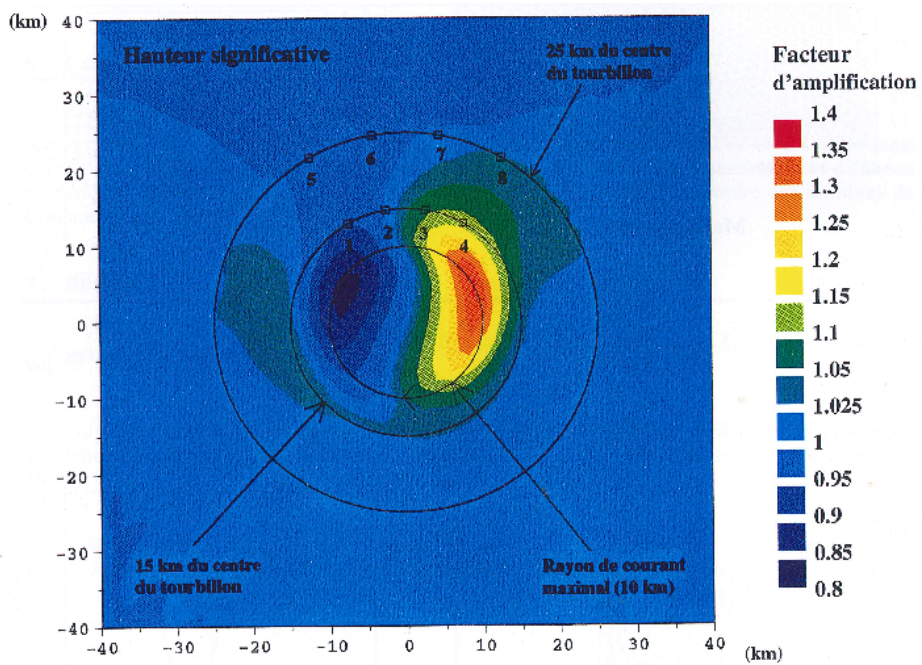


Figure 3.48: significative heighth and positions of the measurement points

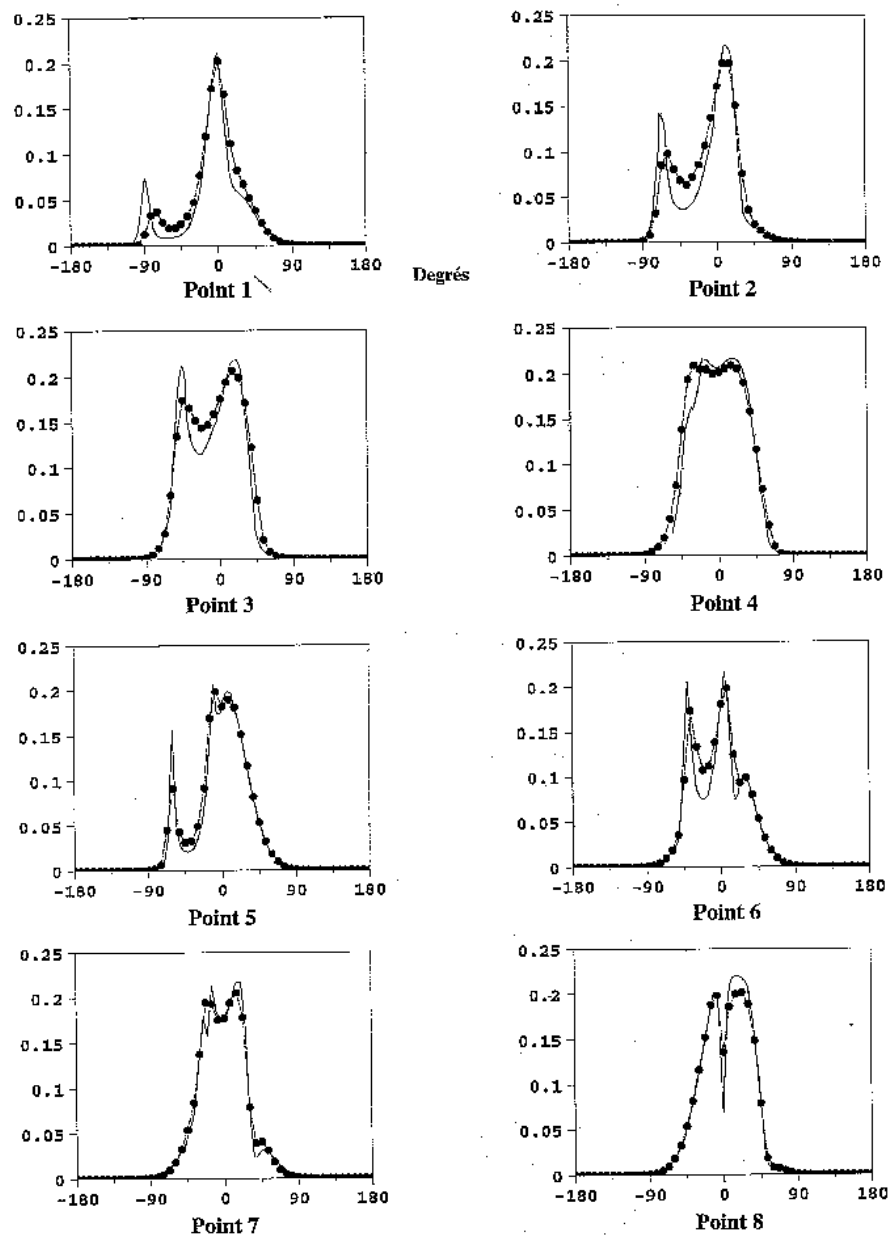


Figure 3.49: Comparison of the angular spread at 0.1 Hz between Tomawac and Mathiesen

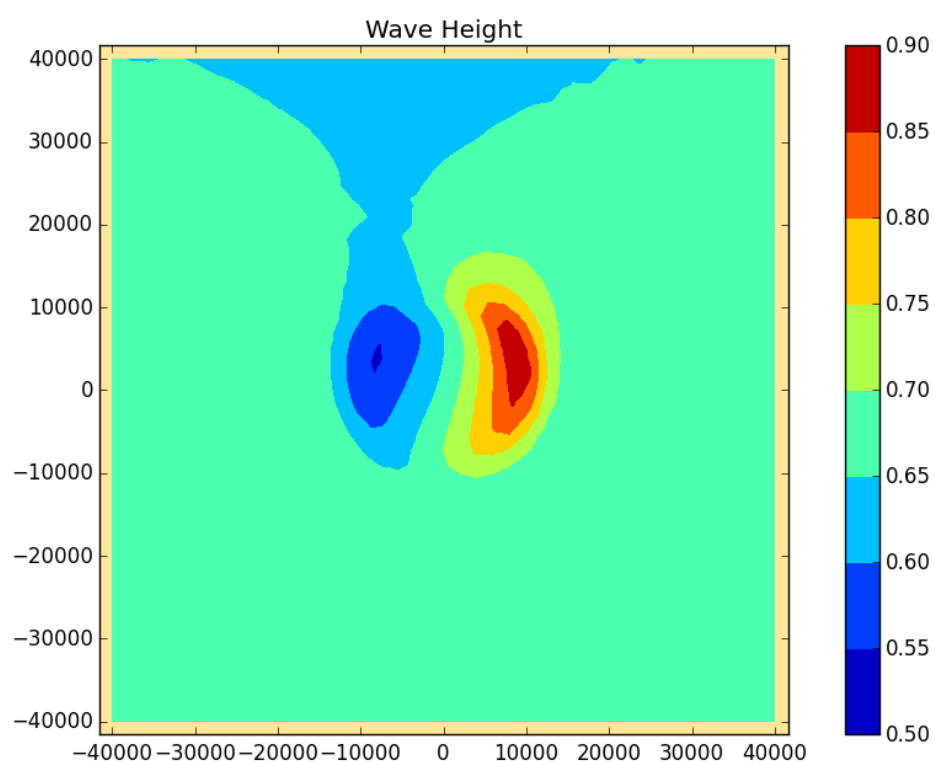


Figure 3.50: significative heighth of the last calculation

- [1] BANNER M.L. ALVES J.H.G.M. Revisiting the pierson-moskowitz asymptotic limits for fully developed wind waves,. *Journal of Physical Oceanography*,, 33:1301 – 1323, 2003.
- [2] JANSSEN J.P.F.M. BATTJES J.A. Energy loss and set-up due to breaking of random waves. In *Proc. 16th Int. Conf. Coastal Eng.*, pages 569–587., 1978.
- [3] V. Bacchi E. Gagnaire-Renou N. Durand M. Benoit. Wave energy dissipation by vegetation in tomawac. In *21st Telemac- Mascaret User Club Grenoble*, October 2014.
- [4] K.K. KAHMA C J. CALKOEN. Reconciling discrepancies in the observed growth of wind-generated waves. *J. Phys. Oceanogr.*, 22:1389–1405, 1992.
- [5] Coastal Engineering Research Center (CERC), editor. *Shore Protection Manual*. USACE, Vicksburg, MS, 1977.
- [6] Coastal Engineering Research Center (CERC), editor. *Shore Protection Manual Volume 1*. USACE, Vicksburg, MS, 1984.
- [7] R.G Dean. Equilibrium beach profiles: characteristics and applications. *Journal of Coastal Research*, 7:53–84, 1991.
- [8] Van der WESTHUYSEN A. J. Spectral modeling of wave dissipation on negative current gradients. *Coastal Eng*, 58:17–30, 2012.
- [9] Forget Ph. Gagnaire-Renou E., Benoit M. Ocean wave spectrum properties as derived from quasi-exact computations of nonlinear wave-wave interactions. *J. Geophys. Res. C (Oceans)*, 115, C12, C12058, 2010. doi: 10.1029/2009JC005665.
- [10] HASSELMANN K. BARNETT T.P. BOUWS E. CARLSON H. CARTWRIGHT D.E. ENKE K. EWING J.A. GIENAPP H. HASSELMANN D.E. KRUSEMAN P. MEERBURG A. MULLER P. OLBERS D.J. RICHTER K. SELL W. WALDEN H. Measurements of wind-wave growth and swell decay during the joint north sea wave project (jonswap). *Deutschen Hydrographischen Zeitschrift*, 8 N 12, 1973.
- [11] GABRIEL D HEDGES TS, ANASTASIOU K. Interaction of random waves and currents. *Waterway Port Coastal and Ocean Engineering*, 111:275–288, 1985.
- [12] TOLMAN H.L. A third-generation model for wind waves on slowly varying unsteady and inhomogeneous depths and currents. *J. Phys. Oceanogr.*, 21:782–797, 1991.
- [13] LAVRENOV I.V. Effect of wind wave parameter fluctuation on the nonlinear spectrum evolution. *J. Phys. Oceanogr.*, 31:861–873, 2001.

- [14] HASSELMANN K. KOMEN G.J., HASSELMANN S. On the existence of a fully developed wind-sea spectrum. *J. Phys. Oceanogr.*, 14:1271–1285, 1984.
- [15] YAN L. An improved wind input source term for third generation ocean wave modelling. Tech. Rep., 8, Royal Dutch Meteor. Inst, 1987.
- [16] HUANG N.E. LAI RJ, LONG SR. Laboratory studies of wave-current interaction : kinematics of the strong interaction. *Journal of Geophysical Research*, 94:16201–16214, 1989.
- [17] BENOIT M. Logiciel tomawac de modélisation des états de mer en éléments finis. dossier de validation de la version 1.0. Technical Report HE-42/96/010/B, EDF-R&D-LNH, 1996. Fiche cas-test : Evolution du spectre directionnel de houle dans un vent tournant.
- [18] MATHIESSEN M. Wave refraction by a current whirl. *Journal of Geophysical Research*, 92:3905–3912, 1987.
- [19] Thellier P. Marcos F. Benoit M. Cowadis software for finite element wave propagation in coastal areas : Validation document of release 1.0. Technical report, EDF R&D, 1998.
- [20] T. Suzuki M. Zijlema B. Burger M. C. Meijer and S. Narayan. Wave dissipation by vegetation with layer schematisation in swan. *Coast. Eng.*, 59:64–71, 2011.
- [21] F. M. Mendez and I. J. Losada. An empirical model to estimate the propagation of random breaking and nonbreaking waves over vegetation fields. *Coast. Eng.*, 51:103–118, 2004.
- [22] JANSSEN P.A.E.M. Wave-induced stress and the drag of air flow over sea waves. *J. Phys. Oceanogr.*, 19:745–754, 1989.
- [23] JANSSEN P.A.E.M. Quasi-linear theory of wind-wave generation applied to wave forecasting. *J. Phys. Oceanogr.*, 21:1631–1642, 1991.
- [24] VAN VLEDDER G. Ph. *Directional response of wind waves to turning winds*. PhD thesis, Delft University of Technology, 1990.
- [25] SNYDER. R.L. DOBSON F.W. ELLIOT J.A. LONG R.B. Array measurements of atmospheric pressure fluctuations above surface gravity waves. *J. Fluid Mech.*, 102:1–59, 1981.
- [26] BATTJES J.A. Van der WESTHUYSEN A. J., ZIJLEMA M. Nonlinear saturation-based whitecapping dissipation in swan for deep and shallow water. *Coastal Eng.*, 54:151–170, 2007.
- [27] BRIGGS M.J. VINCENT C.L. Refraction-diffraction of irregular waves over a mound. *Journal os Waterway, Port, Coastal and Ocean Engineering*, 115 N2:269–284, 1989.
- [28] B W. WILSON. Numerical prediction of ocean waves in the north atlantic for december 1959. *Deutsche Hydrographische Zeitschrift*, 18 (3):114–130, 1965.
- [29] K. P. Hubbert J. Wolf. Numerical investigation of depth and current refraction of waves. *Journal of Geophysical Research*, 96:2737–2748, 1991.